TÉCNICO LISBOA

Battery State of Charge Monitor for Internet of Things Devices

Pedro Miguel Mateus Coutinho

Thesis to obtain the Master of Science Degree in

Electronics Engineering

Supervisor: Prof. Luís Filipe Soldado Granadeiro Rosado

Examination Committee

Chairperson: Prof. Paulo Ferreira Godinho Flores

Supervisor: Prof. Luís Filipe Soldado Granadeiro Rosado

Member of the Committee: Prof. Francisco André Corrêa Alegria

October 2021

Declaration

I declare that this document is an original work of my own authorship and that it fulfills all the requirements of the Code of Conduct and Good Practices of the Universidade de Lisboa.

Declaração

Declaro que o presente documento é um trabalho original da minha autoria e que cumpre todos os requisitos do Código de Conduta e Boas Práticas da Universidade de Lisboa.

Abstract

Batteries are responsible for converting efficiently and safely electrical to chemical energy, and vice-versa, to power wireless Internet of Things devices. These charge storage devices depend heavily on certain factors such as: operational temperature; discharging current; safety precautions; and ease of access. Primary batteries are non-rechargeable power sources with prominence on the alkaline and lithium-iron disulfide types since these are two equally-shaped batteries.

The Internet of Things (IoT) is a set of programmable devices that interact with each other and can be accessed in real time from a remote location depending on the type of network used.

The state of charge (SOC) is a key indicator responsible for stating a percentual remaining charge capacity of a battery. There are several SOC estimation methods that measure this indicator in different ways such as: chemically; using pressure; measuring the open circuit voltage (OCV); measuring the discharged current. The Coulomb counting method is one of the most accurate techniques, designed for all types of batteries, convenient since they don't need to be intervened and may be used simultaneously while measuring the discharged current.

To have the maximum benefit from the new measurement concept, a modified Coulomb counter was developed. Compared with the general circuit of the Coulomb counting method, this new circuit has the same three components: a sense resistor; an operational amplifier; and a counter. Between these two electronic circuits, the new method has distinct electronic components responsible for the current integration that replace the analog-to-digital converter (ADC) of the general circuit: the resistor and capacitor responsible for the current integration; the transistor responsible for charging and discharging the capacitor; and the enhanced comparator that allows the counting between pulses by limiting the capacitor's maximum charging voltage. Together, the maximum error of the SOC estimation is below 3% within the current range from 1 mA up to 110 mA at 20-22ºC with a production cost of 10€.

The main objective of this component replacement is to study another way of measuring current without compromising the measurement accuracy, energy consumption and production cost of the circuit of the Coulomb counting method.

Keywords: Battery; Internet of Things; State of Charge; Coulomb Counting.

Resumo

As baterias são responsáveis por converter energia elétrica em química, e vice-versa, de forma eficiente e segura para alimentar energeticamente dispositivos Internet das Coisas sem fio. Estes dispositivos de armazenamento de energia dependem fortemente de certos fatores como: a temperatura operacional; a descarga de corrente; precauções de segurança; e facilidade de acesso. As baterias primárias são fontes de energia não recarregáveis com destaque nas baterias alcalinas e de lítio ferro, uma vez que são duas baterias de formato igual.

A Internet das Coisas (IoT) é um conjunto de dispositivos programáveis que interagem entre si e podem ser acedidos remotamente dependendo do tipo de rede utilizado.

O estado de carga (SOC) é o indicador responsável por indicar a capacidade percentual da carga restante duma bateria. Existem vários métodos de estimativa de SOC que medem este indicador de diferentes maneiras, tais como: quimicamente; usando pressão; medindo a tensão do circuito aberto; ou medindo a corrente descarregada. O método de contagem de Coulomb é uma das técnicas mais precisas, projetada para todos os tipos de baterias, e pode ser usado em simultâneo com a medição da corrente descarregada.

De modo a beneficiar ao máximo do novo conceito de medição, foi desenvolvido a abordagem da integração de Coulomb. Comparado com o circuito geral deste método, o novo circuito tem os mesmos dois componentes: uma resistência de deteção e um amplificador operacional. Entre estes dois circuitos eletrónicos, o novo método possui distintos componentes responsáveis pela integração da corrente que substituem o conversor analógico-digital (ADC) do circuito geral: a resistência e o condensador responsáveis pela integração da corrente; o transístor responsável por carregar e descarregar o condensador; e o comparador que, limitando a tensão máxima de carga no condensador, possibilita a contagem da duração entre impulsos. Juntos, o erro máximo da estimativa do SOC é inferior a 3% dentro do alcance de medição de 1 mA até 100 mA a 20-22ºC com um custo de produção aproximadamente igual a 10 €.

O objetivo principal é estudar uma nova abordagem de medição de corrente sem comprometer a precisão da medição, o consumo de energia e o custo de produção do circuito do método de contagem de Coulomb.

Palavras-chave: Bateria; Internet das Coisas; Estado de Carga; Contagem de Coulomb.

Contents

List of Figures

List of Tables

Acronyms

ADC	Analog to Digital Converter
DAQ	Data Acquisition System
eCOMP	Enhanced Comparator
FET	Field Effect Transistor
GUI	Graphical User Interface
LPWAN	Low Power Wide Area Networks
OCV	Open Circuit Voltage
Op-amp	Operational Amplifier
PCB	Printed Circuit Board
PDS	Percentage Drop per Sample
PTC	Positive Temperature Coefficient
SOH	State of Health
RFID	Radio Frequency Identification
RTC	Real-Time Clock
UI	User Interface

Acknowledgements

In this chapter, I would like to express my thankfulness and appreciation to the people that helped me throughout these five years at Instituto Superior Técnico and on the elaboration of this dissertation. This document represents the final step of my journey as a student, and I dedicate this work to all because without you it would not be possible.

I want to express thanks to my five colleagues and close friends André Oliveira, Hugo Cunha, Miguel Andrade, Markiyan Pyekh and Sara Soares for all the support regarding programming, electronic assembly, and work we had during our dissertations and throughout these five years at Instituto Superior Técnico. Working with you has been an extremely valuable experience and enjoyable time.

A special thanks to my supervisor Professor Luís Rosado for the outstanding support, guidance, and helpful suggestions throughout the elaboration of my dissertation. Without your advice, constructive criticism, and encouragement I could not have made this far.

I would like to show my appreciation to my girlfriend Joana Moreira and best friend António Rouxinol for the motivation and patience when it was most required.

To my family, my parents António and Susana, my sister Sara and brother António. I thank them for the unconditional support and encouragement.

And lastly, I would like to thank the *Instituto de Telecomunicações* for the conditions and materials provided for the completion of the dissertation.

1. Introduction

Introduction

1.1 Purpose and Motivation

The Internet of Things (IoT) is a system that incorporates smart devices that bring the social, technical, and economical benefits to our everyday life and is based on technological advances and visions of network ubiquity that are enabled anytime, anyplace for anything and anyone [1]. Currently, a great extent of devices is connected to the IoT, and these can have a wired or battery powered source. In this document, various types of batteries including their different chemical compositions are discussed although the disposable alkaline and lithium iron disulfide batteries are emphasized due to their popularity amongst IoT devices. Alkaline batteries are more used in devices used sporadically such as TV remotes, computer mice and flashlights as these require low current, aren't in continuous discharge and, differently from lithium batteries, are safer and more affordable [2]. Lithium iron disulfide batteries have unique properties that have made them as the power source for consumer electronics of high tech market since they are considered the world's longest lasting batteries [3]. They are characterized by supporting high discharge currents, being light weight, having high charge density, long shelf life, and can work in a wide temperature range that can be found on devices such as drones, cameras, and gaming systems [4][5].

The aim of this project is to develop a new circuit capable of estimating a percentual value of the remaining battery life, the state of charge (SOC), of IoT devices by continuously monitoring this indicator using the Coulomb counting method. Based on the SOC estimates, it is possible to predict the various types of battery behaviors according to factors such as temperature variations, charging with different input voltages, endurance of a single charge and lifespan. Temperature is one of the factors that the batteries' performance depends most. Overheating affects charging, endurance and mostly the battery's lifespan. Charges with excessively high input voltages as well as high current discharges are also detrimental to the performance of a battery due to chemical and temperature factors. Therefore, the endurance of a battery depends on its type, the temperature that it is operating, the device's voltage requirement and the wattage that it is charged and discharged.

Deploying IoT battery-powered devices creates a challenge on supervising the maintenance of batteries. IoT devices commonly use non-rechargeable batteries and the device's power management systems must have an ultra-low power consumption to guarantee an extended and efficient operating lifetime. The Coulomb counting method is one of the most accurate and power efficient methods on estimating the SOC of batteries. The main objective of the modified method on current integrating is to study a new approach of measuring current maintaining the accuracy of the measurement, power consumption and production cost of the circuit of the Coulomb counting method.

1.2 Objectives

The aim of the project is to study and formulate an electronic circuit that monitors the state of charge of disposable alkaline batteries and lithium iron disulfide batteries. For this, it is necessary to:

- develop an alternative circuit of the Coulomb counting technique, explaining its accuracy, its energy consumption, and the complexity of the circuit;
- develop a state of charge (SOC) monitor that returns value of this indicator using the modified Coulomb counting approach;
- test and create graphical representations of the SOC and voltage acquisitions side by side with different types of batteries.

1.3 Document's Organization

This document has five chapters, the content of which is described below.

Having described all the intentions and project's goals in the first chapter, the second section is the state of the art in which the general concepts of batteries, state of charge, state of health, IoT devices, Coulomb counting method, commercial solutions and battery capacity dependency are defined.

The third chapter is the development of the proposed Coulomb integrator describing the necessary for the implementation requirements, system's design, the hardware assembly and software for the microcontroller, production cost, user interface and battery capacity estimates.

The fourth section has all the experimental results of the implemented measurement system, this is, the characterization, expected and validation results as well as its energy consumption analysis.

The fifth and final section is a summary of the conclusions of this project with all the achievements and final thoughts. This chapter additionally discusses the advantages and drawbacks of the proposed method compared to the conventional one as well as recommendations for its usage and future work.

2. State of the Art

State of the Art

2.1 Battery Chemistry

A battery is a power source that is able to store and supply charge by converting electrical energy to chemical and vice-versa. The growing demand for energy storage encourages the growth of high-performance batteries. Previously, the most common batteries in low power IoT devices were alkaline, however, the disposable lithium iron disulfide batteries are currently preferably chosen for some cases since they deliver different features maintaining the same shapes and sizes. In this project, these are the two types of batteries studied and, in this section, important concepts of these energy storage devices are mentioned as well as its chemistry, common types, advantages and drawbacks.

A cell is an electrochemical component that contains the electrodes, a separator, and an electrolyte while a battery is a group of cells with housing, electrical connections, and, in some cases, a protective electronic circuit [6]. The electrodes correspond to the conductive part in contact with a material of less conductivity responsible for exchanging positive or negative charge carriers. Demonstrated in Figure 2.1.1, the electrons are the negative charge that flow from the negative to the positive electrodes, anode, and cathode, respectively. On the other hand, the electrolyte is a substance that enables the flow of these electrons, responsible for separating the anode from the cathode preventing the electrodes from being in contact with each other.

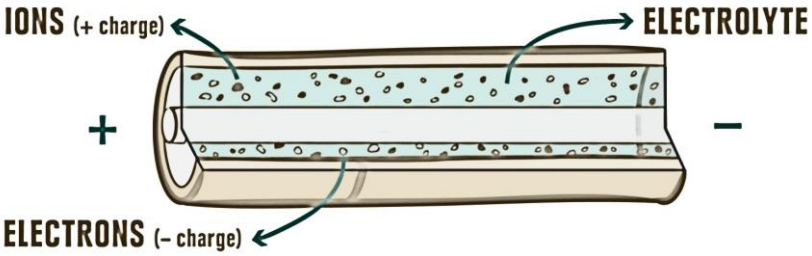

Figure 2.1.1 - Inside a common battery [8].

In the anode, a reaction occurs between the electrode and the electrolyte producing electrons which remain stored at the anode. Simultaneously, another chemical reaction occurs at the cathode enabling this electrode to accept electrons. Therefore, batteries are devices that convert chemical energy into electrical energy through an electrochemical oxidation-reduction (redox) reaction. These are closed systems in which the anodes and cathodes are responsible for the charge transfer and those that play the main role in the redox reaction [6].

Batteries work in two different mechanisms, the charge and discharge mechanism. In the first, the battery receives electrical energy and converts that energy chemically to move electrons from the cathode to the anode. The second mechanism consists of an operation in which the battery supplies electrical energy by electrons from the anode to the cathode, illustrated in Figure 2.1.2 [7].

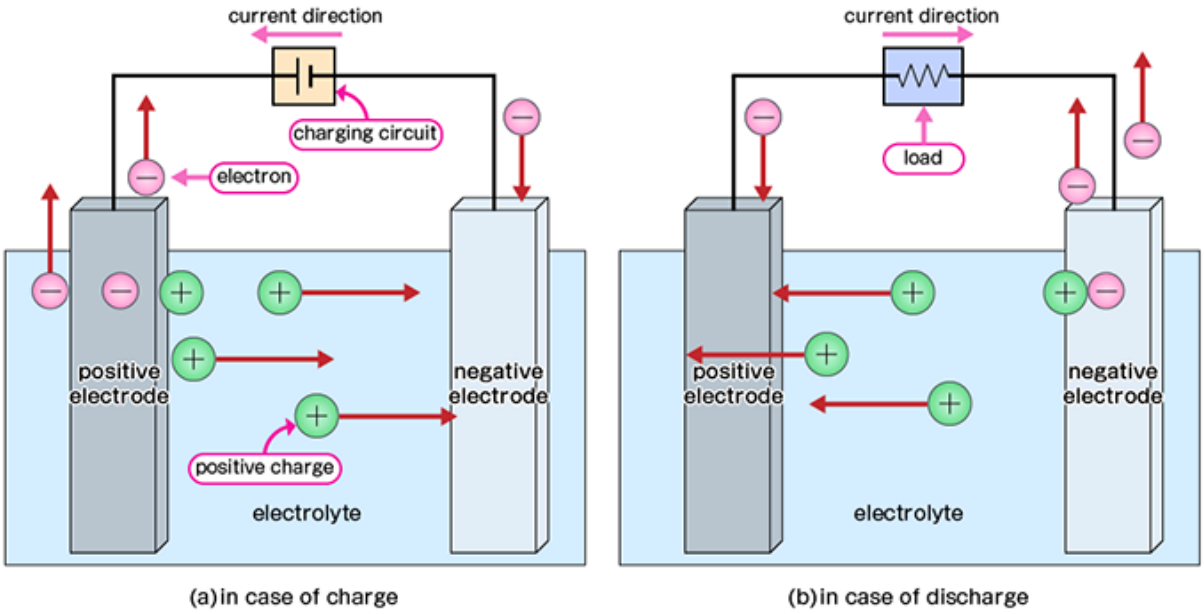

Figure 2.1.2 - Charge and discharge mechanisms [6].

There are two types of voltaic batteries: primary and secondary. The primary ones are all types of non-rechargeable batteries, while the secondary ones are the batteries designed to be rechargeable. A primary battery is a galvanic battery intended for one time usage due to its non-reversible electrochemical reaction inside the battery. Several characteristics should be considered when choosing a battery such as: the initial and life-cycle costs; rechargeable or non-rechargeable; operating temperature; operating voltage; size, design, and weight.

The Figure 2.1.3 illustrates five common battery designs and sizes used in most IoT and non-IoT devices. These letters are indicators of size and voltage output. The further moving along the alphabet letters, the larger are these two variables and if a letter is used more than once, than the smaller it size. For example, PP3 has more voltage output than D and AAA is smaller than AA. Illustrated in Figure 2.1.3, in these five energy storage devices, only the AAA, AA and PP3 (9-Volt) batteries are specifically characterized and studied for alkaline batteries however only AA and AAA for lithium-iron due to not existing the typical 9 V lithium-iron batteries [8].

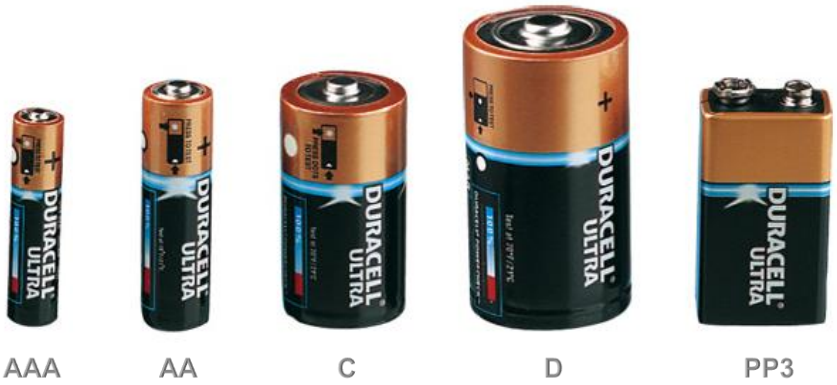

Figure 2.1.3 - Illustration of the five most common batteries [28].

As the resources responsible for the chemical reaction are depleted, the voltage of a battery is gradually reduced over its lifetime. Devices will only function normally in a certain voltage range that they were intended to work on, so after some usage, a battery will not be able to power it normally. Certain factors can make a battery less efficient as well as affecting its lifetime: low temperatures inhibit the ions' movement and, consequently, lowers the battery's efficiency; high current drainage reduces the battery capacity because with higher current, the less time there is for the chemical reactions to occur and consequently less energy may be discharged from the battery.

Batteries gradually loose its ability to provide the same nominal voltage over time due to usage and its current loss called, self-discharge. Naturally, the lower the self-discharge, the better outcome for the battery life. Certain considerations as the temperature the device is operating are directly related to the self-discharge, doubling its value for every 10°C higher than the ambient 20°C temperature [9].

2.1.1 Alkaline Batteries

An alkaline battery is composed by an alkaline potassium hydroxide (KOH) electrolyte and can be rechargeable or non-rechargeable. The cathode is a compound of magnesium dioxide (MnO_2) while the anode is zinc (Zn). Illustrated in Figure 2.1.4, the battery has a positive connection at the top and a negative connection at the bottom [10]. The cylinder has an outer coating and an ion conducting separator that keeps the two electrodes apart. Inside the battery, there is zinc that is separated from the cathode by an ion-conducting separator. The anode is in contact with a current pick up that is connected to the negative terminal of the battery. This device is protected at the bottom by a protective cover and a cellar to expand the pressure at the bottom.

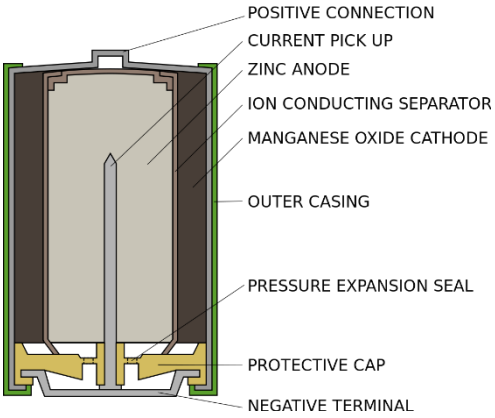

Figure 2.1.4 - Inside an alkaline battery [5].

The oxidation reaction is when the substance gains electrons,

$$\mathrm{Zn(s) + 2OH^-(aq) \rightarrow ZnO(s) + H_2O(l) + 2e^-.} \quad (1)$$

Otherwise, the reduction reaction occurs, which is when the substance loses electrons,

$$\mathrm{2MnO_2(s) + H_2O(l) + 2e^- \rightarrow Mn_2O_3(s) + 2OH^-(aq)} \quad (2)$$

and the overall reaction of an alkaline battery being,

$$\mathrm{Zn(s) + 2MnO_2(s) \rightarrow ZnO(s) + Mn_2O_3(s).} \quad (3)$$

Alkaline batteries are susceptible to leaking their electrolyte due to attempts on recharging, combining different battery chemistries to power the same circuit or storing batteries in humid places with peak temperatures. The contact with the potassium hydroxide chemical may cause respiratory, eye and skin irritation, however, compared to other types of batteries, the alkaline batteries are considered safe. The magnesium dioxide is the first chemical to run out, therefore no more electrons are released after this cathode compound is over.

Two main factors can make a battery less efficient as well as affecting its lifetime: low temperatures and higher discharge currents. Thus, these types of energy storing devices are usually used for devices that generally have low supply current and where certain factors such as weight, size and energy density are not deal breakers.

2.1.2 Lithium Iron Disulfide Batteries

Lithium batteries are another type of batteries widely used in electronic devices with a major advantage over alkaline for being more energetically dense. In lithium batteries, there are two common types of batteries: lithium-ion and lithium iron. These are distinguished by their energy density, charging time and overall safety. Lithium iron disulfide batteries are heavier and bulkier in size than lithium-ion batteries though being longer lasting [11][3]. In this project, lithium iron disulfide ($LiFeS_2$) batteries are studied for being very similar to alkaline cells since they are disposable and share the same shapes and sizes.

Unlike alkaline primary batteries, a lithium iron disulfide cell is chemically different having a spiral structure with two very thin layers of electrodes wrapped in a so-called “jellyroll” cylindrical shape, illustrated in Figure 2.1.5 bellow, having 20 times more surface area. Lithium is the lightest and most active metal and, when in contact with iron disulfide, it can supply the energy needed for most electronic devices with a nominal voltage of 1.5 V for AA and AAA batteries.

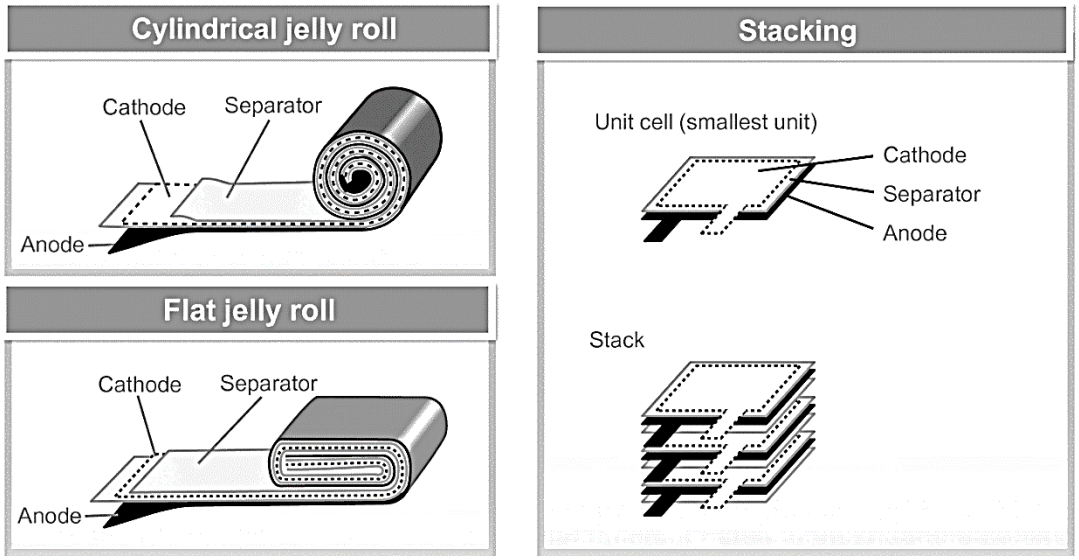

Figure 2.1.5 - Cylindrical and flat jelly rolls compared to stacking designs [29].

The electrodes of a lithium iron disulfide cell are separated by a microporous membrane that allows the ions to move freely during normal use. The non-aqueous electrolyte of these batteries is designed to work with wide temperature ranges from -40ºC to 60ºC [12]. Like the alkaline batteries, the voltage of the lithium metal ones also gradually reduces over time once the resources responsible for the chemical reaction are depleted.

The overall chemical reaction inside the cells takes place in two steps. In the first step,

$$2\mathrm{Li} + \mathrm{FeS_2} \rightarrow \mathrm{Li_2FeS_2} \quad (4)$$

and the second discharge step is,

$$2\mathrm{Li} + \mathrm{Li_2FeS_2} \rightarrow \mathrm{Fe} + 2\mathrm{Li_2S}. \quad (5)$$

These cylindrical batteries have lithium as anode, iron disulfide as cathode and, between these two electrodes, the electrolyte is an organic solvent blend of lithium salt, demonstrated in Figure 2.1.6.

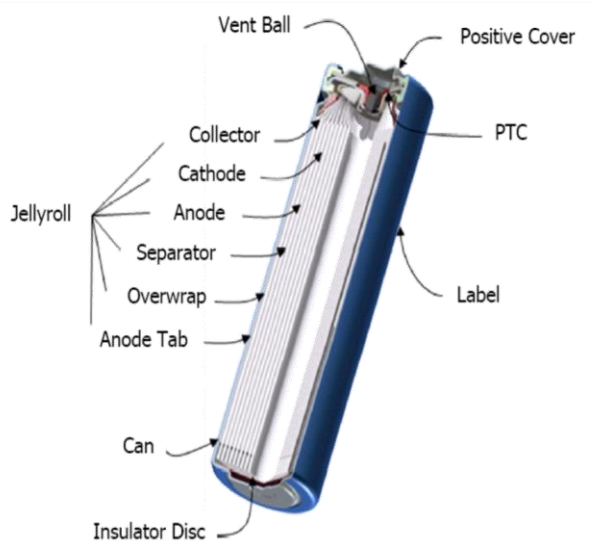

Figure 2.1.6 - Typical cylindrical lithium iron disulfide battery

The vent ball is a safety mechanism capable of releasing some pressure off the battery. The positive and negative contact covers are nickel plated steel surfaces, and the non-conductive plastic film label is responsible the isolation of the battery. The Positive Temperature Coefficient (PTC) is a safety device placed inside the battery responsible for reversibly shut it down at high temperatures. Lithium iron disulfide batteries are less sensitive to temperature than alkaline though the service life is still affected if the temperature is lowered below room temperature (20ºC) [12].

2.1.3 Advantages and Disadvantages

Choosing a type of battery for an electronic device is important because every type has its drawbacks, though, there is always a better choice depending on its purpose. Briefly, some advantages of using lithium iron disulfide over alkaline and vice-versa are listed below and, in Table 2.1.1, a summed-up comparison between these two batteries in different characteristics is made.

The lithium iron disulfide ($LiFeS_2$) cells are better than the alkaline ones [12] for having:

- significantly more power to deliver;
- longer service in mild to heavy current drainage or in low temperatures applications;
- greater operating voltage and flatter discharge curve;
- more endurance to leakage and better service maintenance when stored;
- substantially lighter and energetically denser.

Nevertheless, alkaline batteries are still better in some cases since they are more budget friendly, do not have transportation concerns like lithium batteries have, and, although lithium batteries have the PTC device inside them, alkaline cells are still much safer.

Table 2.1.1 - Alkaline and lithium iron batteries' comparison [12].

Characteristics	Lithium Iron	Alkaline
Cold Temperature Performance	Superior	Good
Weight	33% < Alkaline	33% > Lithium
Shelf Life	20+ Years	5 to 10 Years
Leakage	Superior	Good
Discharge Curve	Flat	Sloping
High Rate Capability	Superior	Good
Safety	Concerning	Safe
Price	High	Low

2.2 Battery Indicators

2.2.1 State of Charge

The state of charge (SOC) is the level of charge remaining in a battery and it is the quotient between the amount of payload and the total capacity of the battery. The payload, Q(t), is the total amount of charge remaining in a battery and, Q_n, is a pre-determined value considered as the maximum usable [13]. The SOC is expressed as a percentage,

$$\mathrm{SOC}\,(t) = \frac{Q\,(t)}{Q_n} \times 100\ [\%]. \tag{6}$$

That is, SOC is 0% on an empty battery and 100% on a fully charged one. Generally, there are four common SOC estimation techniques that may be used depending on the types of applications required: Chemical; Voltage; Pressure; Coulomb counter. As stated in the Table 2.2.1, in all these methods there are advantages and drawbacks and depending on the applications there are some preferable approaches to use than others [14].

The chemical method works only on batteries that allow an access to its electrolyte. This can be seen on non-sealed lead acid batteries for example and the specific gravity (SG) of this substance is used to stipulate the battery's SOC. Based on the concept of buoyancy, a hydrometer is the instrument used to determine the SG of a battery that it is directly compared to the corresponding SOC. This technique has shown to be viable although it needs direct access to the battery's electrolyte.

The open circuit voltage (OCV) approach relies on a linear function between the voltage of lead-acid batteries' open circuit and the SOC. On the other hand, unlike these types of batteries, the Lithium-iron disulfate batteries do not have a linear relationship between these two variables. This relationship on LiFe batteries is not the same for all batteries being consequently necessary to estimate the SOC using other methods.

The pressure method is used on certain nickel batteries where its pressure increases when charging and decreases with discharging. The battery contains a gas-tight sealed measurement chamber in which a pressure sensor is assembled [15].

The Coulomb counting approach is a method that precisely measures how much usable charge is available during discharging by comparing it with the battery's previously charged energy [14]. Even though this technique is accurate on measuring current, it needs to measure it continuously. This project will be based on this method, and it is intended to improve some of its aspects as time efficiency and less impact on the battery' performance.

Table 2.2.1 - Overview of some existing techniques for battery SOC [8].

Techniques	Field of Applications	Advantages	Drawbacks
Chemical	Batteries with Electrolyte Access	Easy and Accurate	Works only on batteries that have access to the electrolyte.
Voltage	All Battery Systems	More Accessible	Non-linear relationship between SOC and voltage.
Pressure	NiMH Batteries	Can Also Provide Information About the SOH	Problems on the sensor's stability in the electrolyte and temperature sensitive.
Coulomb Counter	All Battery Systems	Easy and Accurate	Continuous measurement needed and costly.

2.2.2 State of Health

Being only applicable to secondary batteries, the state of health (SOH) is an indicator of the capacity to supply energy throughout a battery' life compared to a new battery. Thus, it serves as a monitor that indicates the battery's performance. During its lifetime, a battery's performance gradually deteriorates due to irreversible physical and chemical modifications caused by its usage and aging. When it indicates 100%, it means that the battery's conditions match the battery's specifications and 80% is usually when manufactures replace a battery with a new one depending on the issued device. There are two commonly used methods to determine the health status of a battery: using the battery's impedance; or using its capacity. For the first method, the SOH is calculated using Equation (7).

$$\mathrm{SOH} = \frac{\mathrm{R_t}}{\mathrm{R_{New}}} \times 100\,[\%]. \tag{7}$$

The resistor R_t is the battery's impedance measured value and the resistor R_{New} is its initial value. On the other method, the SOH is calculated using Equation (8) where C_t is the battery's capacity measurement at the time and C_{New} is the initial value.

$$\mathrm{SOH} = \frac{\mathrm{C_t}}{\mathrm{C_{New}}} \times 100\,[\%]. \tag{8}$$

Although not being the focus of this project, the SOH is a key indicator that provides an estimation of the status of a certain battery inside the consumers device compared to a new one.

2.3 Internet of Things

The Internet of Things (IoT) is a network between devices that can be accessed and controlled in real time from a remote location benefiting users from a broad variety of industries. In this system, sensors, actuators, gadgets, machines and other types of hardware are programmed for certain purposes and interact with each other using the internet or other networks. In Figure 2.3.1, Low Power Wide Area Networks (LPWAN: Sigfox, LoRa, Ingenu), Cellular (3G/4G/5G), Personal Area Network (PAN: NFC, ZigBee, BLE) and Local Area Network (LAN: LoRa, Sigfox, NB-IoT) are four different types of IoT networks that are compared between certain parameters including their bandwidth, power consumption, cost, and range [16].

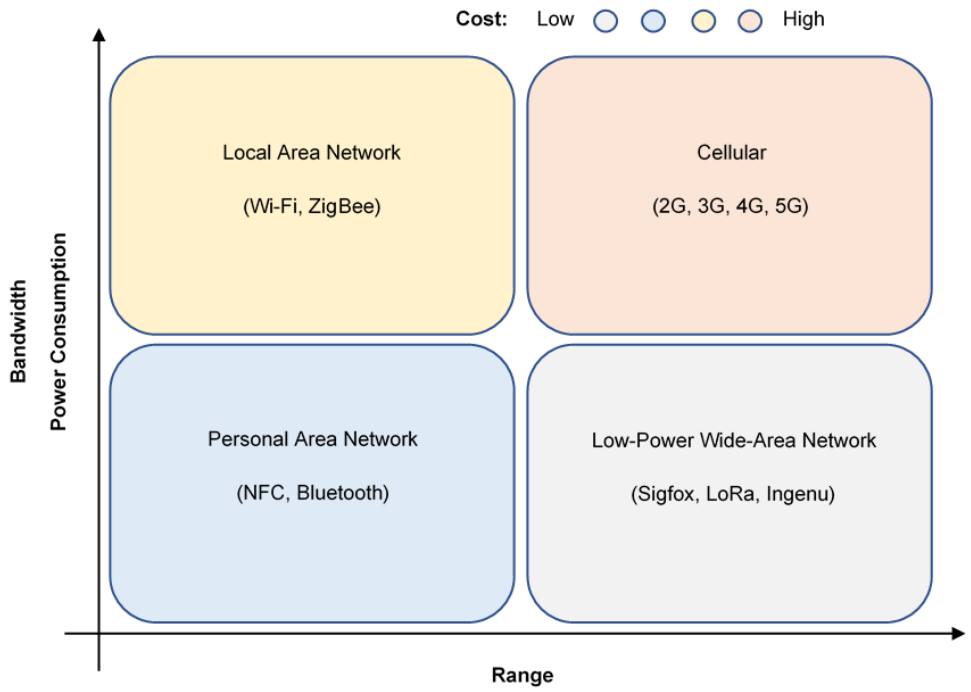

Figure 2.3.1 - Bandwidth, power consumption, cost, and range of different IoT networks.

LPWANs provide long range communication powered by small and inexpensive batteries. However, this leading type of IoT wireless network can only send small blocks of data at a low rate. Cellular networks are one of the most reliable communication protocols in the consumer mobile market as they support an extremely high data rates for long ranges. A major drawback of this broadband communication is the high cost and power needs, and, unlike LPWANs, cellular networks are not viable for some IoT applications. Mesh protocols including Zigbee are short-range and low-power providing higher rates of data compared to LPWANs but, on the downside, it can provide less power-efficiency due to the mesh arrangement. Like Zigbee, Bluetooth is a short-range and low-power network and, despite being more expensive, it is mostly used with electronic devices such as smartphones. Wi-Fi as a crucial role in daily lives due to its extremely high data rate. Nevertheless, its limitations are noticed in terms of coverage, scalability and power consumption not often being the viable solution for a network with several battery-operated IoT sensors. Last but not the least, RFID is a network of small blocks of data transitions from one RFID tag to a reader on a very short range being a relatively cheap protocol.

These devices are usually powered by primary (non-rechargeable) batteries but not some wireless connected IoT gadgets require light, compact, highly dense and with high voltage batteries. For these reasons, secondary batteries (rechargeable) are best suited on devices with these requirements. Choosing the correct battery for the IoT device depends heavily on the device's nominal and cut-off voltage, the environment's temperature and in the type of current pulse of the desired use [17].

Managing the SOC of these stored energy devices can be challenging and knowing that batteries are either primary or secondary, alkaline and lithium iron are the most used for non-rechargeable and lithium-ion are the most used rechargeable batteries for IoT devices. Therefore, the Coulomb counting approach in this project is designed for IoT devices with these two types of batteries.

The SOC is a key indicator for IoT devices since it reflects the performance of their power source, not only for protecting it by preventing over discharge and improving battery life, but also by allowing strategies to save energy [18].

2.4 Coulomb Counting Method

The Coulomb counting is the approach that is the most used and the one chosen for this project as it is easily implemented and directly applied method for measuring and integrating the battery's discharging current over time given by,

$$\mathrm{SOC}\,(t) = \mathrm{SOC}\,(t-1) + \frac{I\,(t)}{Q_n}\,\Delta t. \tag{9}$$

Where SOC (t-1) represents the previous estimated value of SOC, Q_n is the totally charged capacity and I(t) is the discharging current. The Coulomb counting procedure calculates the SOC by accumulating the value of the sourced charge and its accuracy depends mostly on the sampling frequency and the current sensor's accuracy. The SOC is estimated by integrating the charging and discharging currents, initially knowing, or estimating its' value. There are always losses and inaccuracies during charge and discharge processes as the output charge is always less than the stored charge. There are some factors that influence the inaccuracy of the Coulomb counting approach including the battery's temperature, history, discharge current, and life-cycle [19].

The conventional Coulomb charging method, in Figure 2.4.1, measures the SOC by measuring the current flowing in the Rsense resistor with the analog to digital converter (ADC) and storing it with the accumulator and real-time clock (RTC). Comparing this value with the knowing starting point, the SOC can be estimated. However, this method needs a high sampling rate specially when the battery sourced current exhibits fast transients.

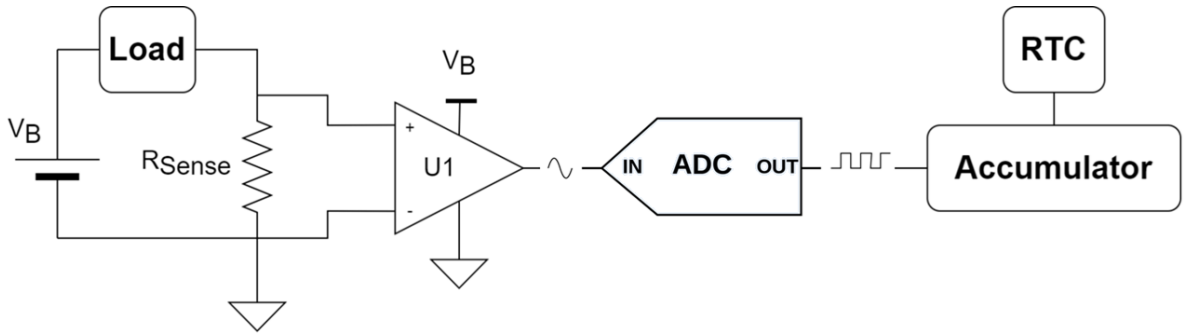

Figure 2.4.1 - The conventional Coulomb counting method.

2.5 Commercial Solutions

There are several improved approaches regarding the Coulomb Counter method that will be discussed in this section. Some commercial solutions include minor adjustments and other have combined two or more well-known methods. These combine the strengths of each method and create a hybrid method to improve the SOC estimation.

2.5.1 Coulomb Counting and Voltage

The Coulomb counter and the Open Circuit Voltage (OCV) are two of the most accurate and precise methods to estimate the SOC [20]. When combined, they form a hybrid model that benefits from the advantages of each improving the SOC estimates [19].

The SOC estimation can be improved by combining the Coulomb counting and voltage methods removing the counting integrator's cumulative error with a calibration of the counter based on the OCV characteristics. It is recommended that the calibration measurement is made when the battery is not discharging high currents due to the battery's internal resistor that causes a voltage drop that significantly compromises the accuracy of the OCV measurement.

The reference nominal value of the battery's capacity needs periodical calibration due to its decrease with age, cycling, operational temperature and discharge current on rechargeable batteries. The calibration of this value is made by charging and discharging the battery at low current rate and updating the maximum charge that it can hold. This hybrid method significantly improves the accuracy of each technique with a lower than 3% error for the duration of a full cell cycling [20]. The main disadvantage of using this alternative method is that the error increases if the battery is continuously used or if the time between charge and discharge cycles is not enough to perform a correct calibration of the maximum capacity value.

2.5.2 Modified Coulomb Counting Method

A modified Coulomb counting method was developed by Wen-Yeau Chang in 2013 intended to improve the conventional Coulomb integrating method [19]. It was noticed a quadratic relationship between the battery's calibrated and measured discharging currents, $I_c(t)$ and $I_m(t)$, respectively,

$$I_c(t) = k_2 I(t)^2 + k_1 I_m(t) + k_0. \quad (10)$$

The constant values, k2, k1 and k0, are calculated previously and used to approximate the measured discharge current with its actual value. Afterwards, in this modified Coulomb counting method, the SOC is calculated with the new corrected current value,

$$SOC(t) = SOC(t-1) + \frac{I_c(t)}{Q_n} \Delta t. \quad (11)$$

Thus, the experimental results made by Wen-Yeau Chang in 2013 reveal an improved accuracy of the modified Coulomb counting method compared to the conventional method.

2.6 Battery Capacity Dependency

It is important to know how a battery operates from an efficiency and safety point of view. The performance of the batteries is strongly affected by several factors, the most important of which are temperature and discharge current. Low temperatures inhibit the ions' movement and, consequently, lowers the battery's efficiency. With higher currents the amount of energy that can be discharged from the battery is reduced and, consequently, its capacity is lower. Some components inside the battery may not have the necessary time for the chemical reaction to occur and so the energy that is discharged is reduced compared to a lower discharge rate [21].

2.6.1 Temperature dependency

The lower the temperature the less movement of ions and, as a result, the less efficient the battery is. Although it affects all battery types, alkaline cells are more sensible to temperature compared to lithium-iron disulfide. In Figure 2.6.1, it is illustrated an example of a graph revealing the temperature effects on a battery capacity with different current values in Energizer AA lithium-iron disulfide cell [22].

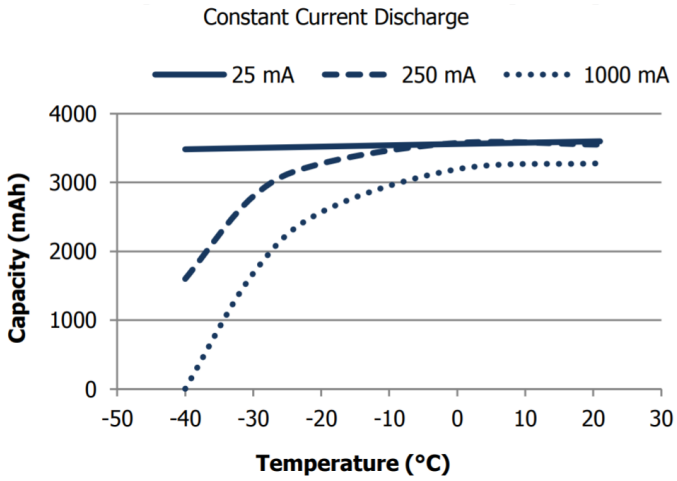

Figure 2.6.1 - Temperature effects on the battery capacity [22].

The temperature's lower limit is determined by the temperature at which the electrolyte freezes, though, as the temperature decreases, performance also decreases. If the temperatures are very high, there may be an expansion and contraction of the components resulting in a negative impact on the battery performance. Alkaline batteries are designed to operate at a range of -18ºC to 55ºC while lithium-iron disulfide can operate at a wider range of -40ºC to 60ºC [22][23].

In these temperature ranges, although the battery capacity is higher with higher temperatures, the battery life is shorter compared to when operating at lower temperatures. For lithium-iron disulfide batteries, for example, when operating at -30ºC, the battery capacity is reduced to about 50% of its nominal value, however the battery life increases up to 60%. On the other hand, at high temperature values, the battery life can be reduced to almost half its designed operating time [24].

2.6.2 Current Dependency

Since the proposed Coulomb Integrator is designed to work at room temperatures rounding 21ºC, a cause that may influence the battery's performance is the discharging current. For this project, current dependency is the most important factor due to affecting the battery life depending on the amount of current drawn. The greater the current is discharged from the battery, the quicker the battery goes flat since less time is given for the chemical reactions to take place and therefore less energy may be discharged from the batteries. Just like on temperature dependency, the capacity of the alkaline batteries has a greater dependency with the current than on the lithium-iron disulfide batteries. In Figure 2.6.2, the capacity of lithium and alkaline batteries are set side by side for performance comparison with different temperature and current values. Alkaline are more sensible to temperature and current drainage due to its greater internal impedance value compared to the lithium.

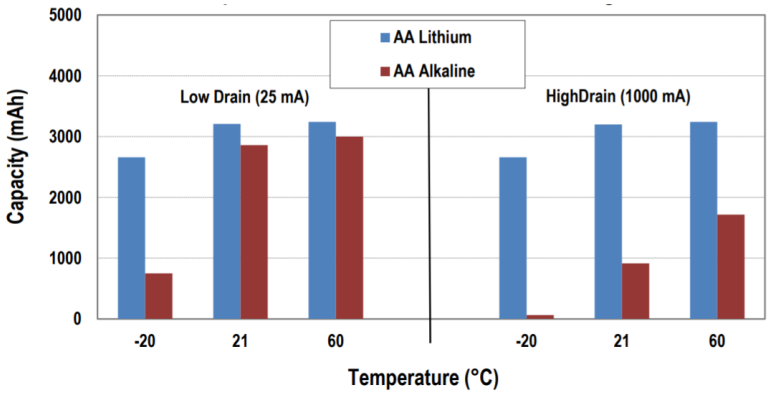

Figure 2.6.2 - AA batteries temperature and discharge current performance [11].

The Figure 2.6.3 illustrates capacity-current dependency of both alkaline and lithium batteries at room temperature [22]. In this project, some tests of the SOC of these batteries were performed at room temperature, about 20-22ºC, and between the range of 1 mA to 100 mA. Therefore, lithium-iron batteries

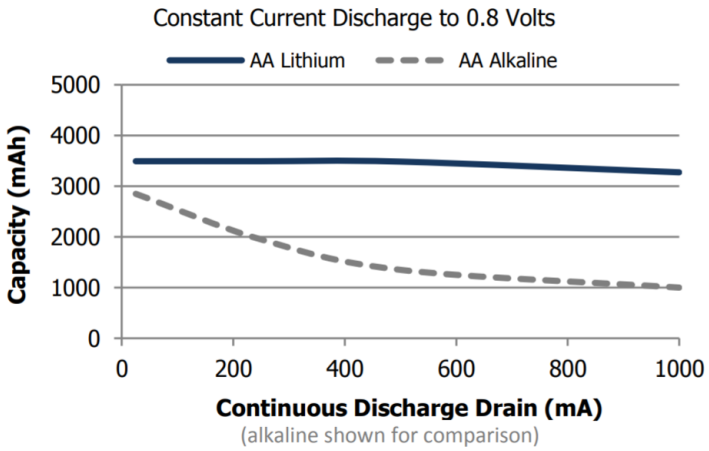

Figure 2.6.3 - Capacity of lithium and alkaline batteries with current discharge [22].

are set as having no current drainage dependency on its nominal capacity. Differently, for alkaline batteries, a function was made to approximate the SOC value dependent on the current requested from the battery.

3. Proposed Coulomb Integrator

Proposed Coulomb Integrator

3.1 Architecture

In this project, an improved technique of the conventional method is proposed with the following circuit represented in Figure 3.1.1. This new approach, Coulomb Integrator, is composed by a NMOS Field Effect Transistor (FET) M1, a capacitor C1, a resistor R1 an operational amplifier (Op-amp) and a Microcontroller MSP430FR2311. In this approach, the SOC is estimated by measuring the current flowing in the Rsense, amplifying the signal with Op-amp, integrating it using a low-pass filter, and comparing the signal with a predefined value of 1 V.

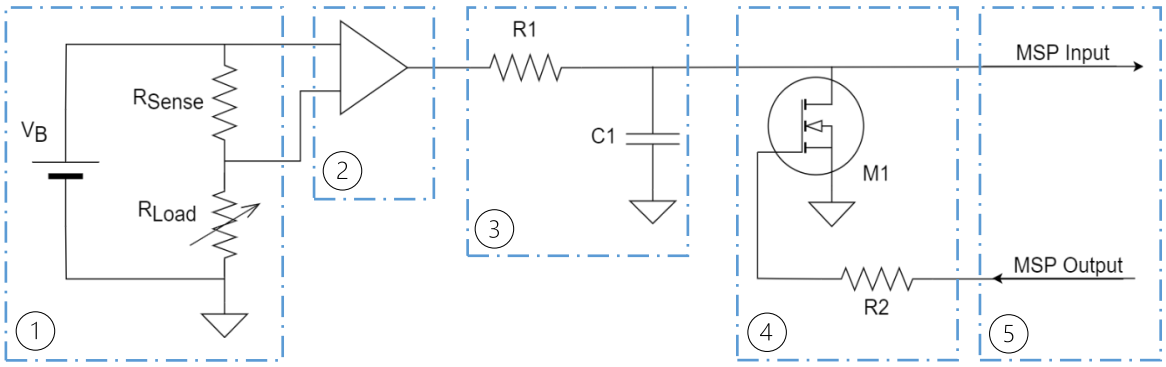

Figure 3.1.1 - Proposed Coulomb counting method.

The first block of this circuit exemplifies a device powered by the battery connected to a sense resistor, Rsense, that must have a significantly lower value compared to the load's impedance because the higher the Rsense impedance, the lower the voltage on the load.

Represented in the second block, the Op-Amp to prevent any influence on the sense and load circuits from the following stages of the architecture, but also for amplifying the Rsense voltage signal that is directly proportional to the desired current value.

In Figure 3.1.2, the values of the voltage of the battery, load, Rsense and Op-Amp output are illustrated in different colors in each block. For example, when the load is being sourced with two 1.5 V battery's discharging 100 mA, on the first block, the green line is the battery's 3 V, the voltage of the Rsense, Vs, is approximately equal to 27 mV and the load's voltage represented in the yellow line is the subtraction between these two: 2.973 V. Then, the second block is the representation of the voltage amplification that occurs inside the Op-Amp. This signal amplifier component has one of the reference voltages connected to ground and the other Vref connected to the microcontroller's 3.3 V. Thus, the output of the Op-Amp is equal to 1.65 V for a 0 V input, half the microcontroller's voltage supply, and 3.3 V for a maximum of 82.5 mV input. Since the gain of this component is equal to 20 V/V, the output voltage of the Op-Amp is,

$$\mathrm{Vop} = \frac{\mathrm{Vref1} + \mathrm{Vref2}}{2} + \mathrm{G} \times \mathrm{Vs}. \tag{12}$$

In this case, for Vs equal to 27 mV, the output is equivalent to 2.19 V represented in the yellow line of the second block,

$$\mathrm{Vop} = 1.65 + 20 \times 0.027 = 2.19\ \mathrm{V}. \tag{13}$$

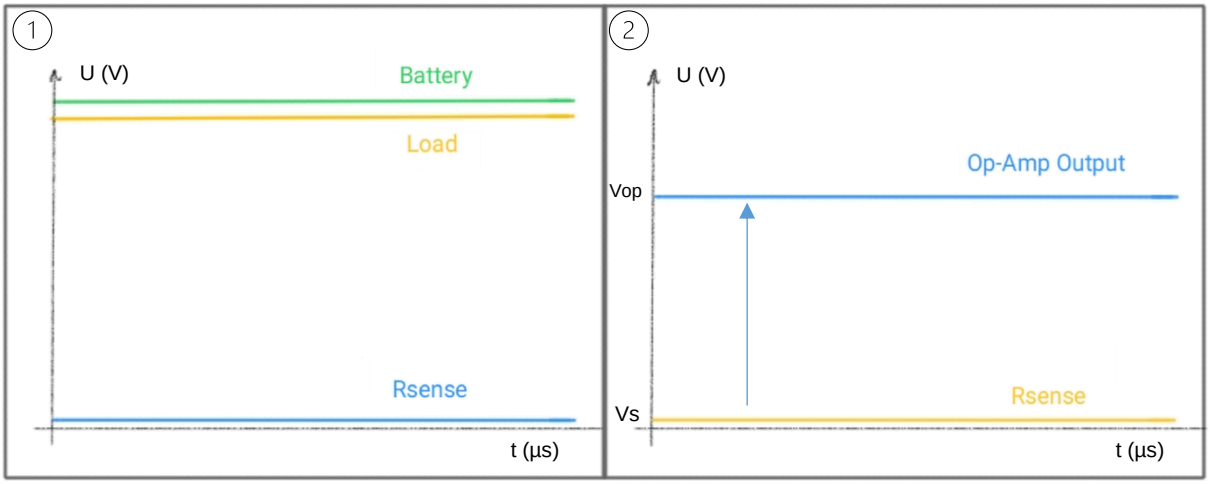

Figure 3.1.2 - Voltage output signal representation of block 1 and 2 with 100 mA.

The third block are the components accountable for integrating the voltage originating a sawtooth waveform output. The transistor M1 from the fourth block is used for discharging the integrator. Demonstrated in Figure 3.1.3 , when the Microcontroller's output is LOW, the capacitor charges and, while it charges, the value of the capacitor's voltage is compared with 1 V inside the Microcontroller. When this input value reaches the compared voltage value, the MSP's output is HIGH, and the transistor discharges the capacitor.

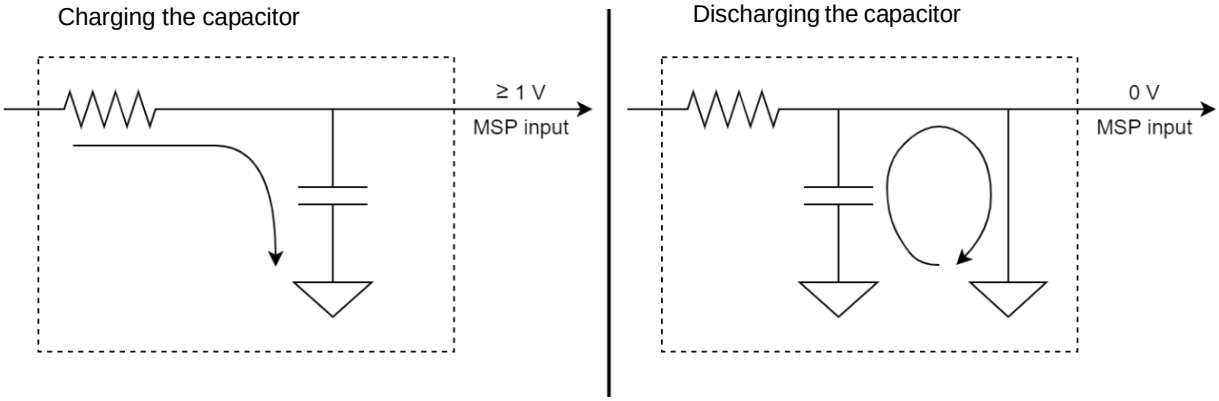

Figure 3.1.3 - Transistor charging and discharging the capacitor illustration.

In Figure 3.1.4, the values of the voltage of the resistor and capacitor are illustrated in yellow and blue, respectively, which characterize the voltage of the components of the integrator from the third block while charging the capacitor. Then, illustrated in the fourth block, since the microcontroller compares the capacitor's voltage in yellow with 1 V, the transistor discharges it every time it reaches this compared V1 value and consequently outputting the sawtooth signal represented in blue.

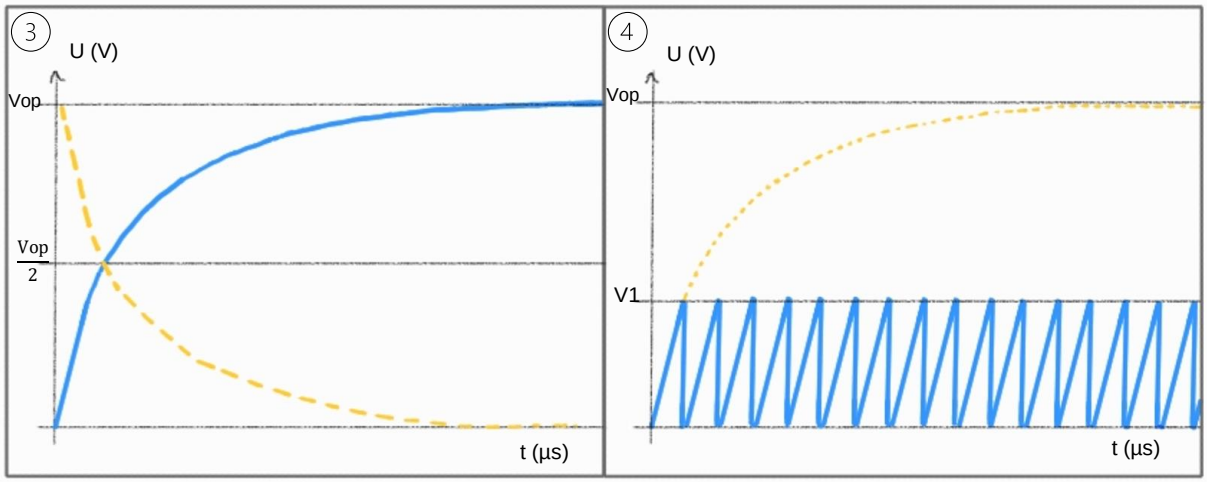

Figure 3.1.4 - Voltage output signal representation of block 3 and 4 with 100 mA.

After the fourth block, illustrated in Figure 3.1.5, the fifth block represents the MSP I/O ports that are connected to the circuit. The yellow line is the input signal of the MSP, and it is connected to one of the comparator's inputs. This internal enhanced comparator (eCOMP) outputs a HIGH voltage, 3.3 V, whenever the input is higher than the comparing value of 1 V, V1, and outputs a LOW voltage, 0 V, whenever it is lower, generating an equivalent pulsed signal represented in blue.

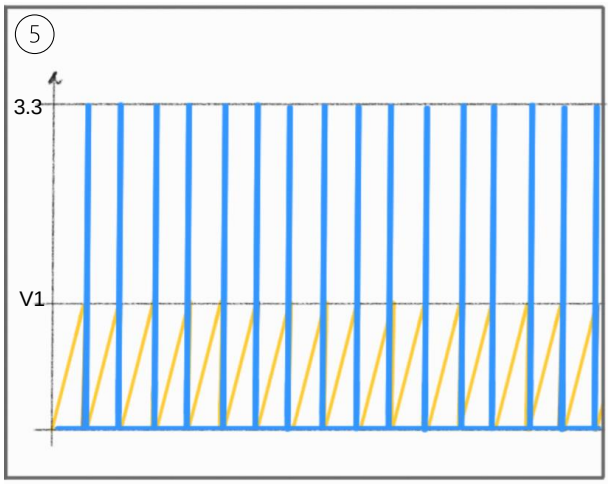

Figure 3.1.5 - Voltage output signal representation of block 5 with 100 mA.

However, if the discharge current is 1 mA, for example, the voltage at the sense resistor is equal to 270 µV. After amplifying the signal, the Op-Amp's output voltage, Vop' is equal to,

$$\mathrm{Vop}' = 1.65 + 20 \times \mathrm{Vs} = 1.66\,\mathrm{V}. \tag{14}$$

Therefore, as show in Figure 3.1.6 of the 1 mA discharge example, in block 4 the yellow line shows the capacitor taking more time to charge completely and, consequently, in blue, the charge until reaching 1 V takes longer than when the battery was discharging at 100 mA. Accordingly, as for block 5, the microcontroller's output pulses are more spaced out between each HIGH output meaning that the counter will count less pulses in the same period compared to the 100 mA discharge.

Lastly, comparing the fifth blocks of the Figure 3.1.5 and Figure 3.1.6, it can be assumed that the higher the value of the discharge current, the higher the number of pulses and the lower the duration between pulses for the same period.

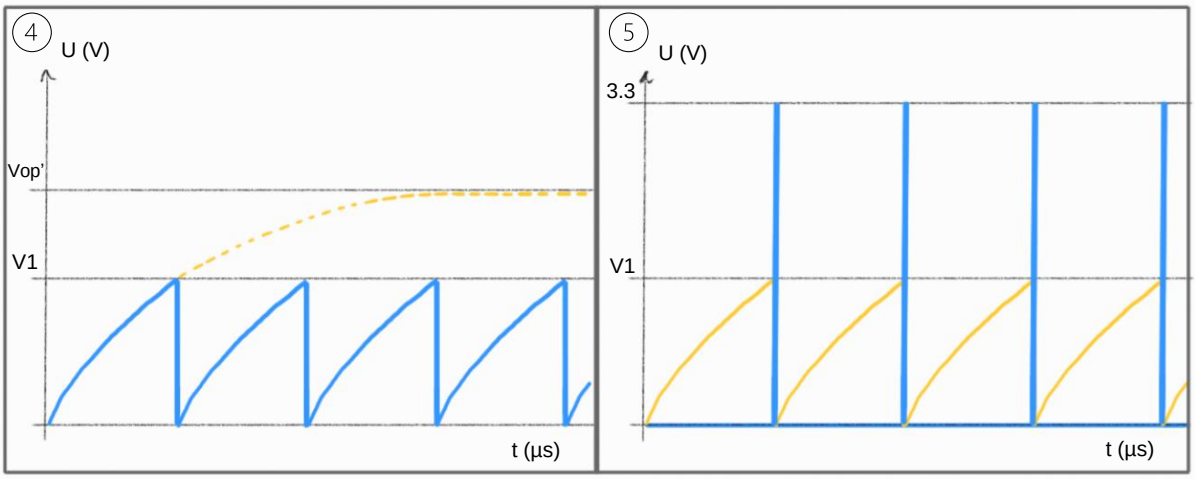

Figure 3.1.6 - Voltage output signal representation of block 4 and 5 with 1 mA.

The Figure 3.1.7 demonstrates a footage of the actual circuit in a breadboard connected to the MSP430FR2311. The RS-200 is the resistor that is simulating the load's impedance and the circuit is being sourced by the microcontroller's 3.3 V.

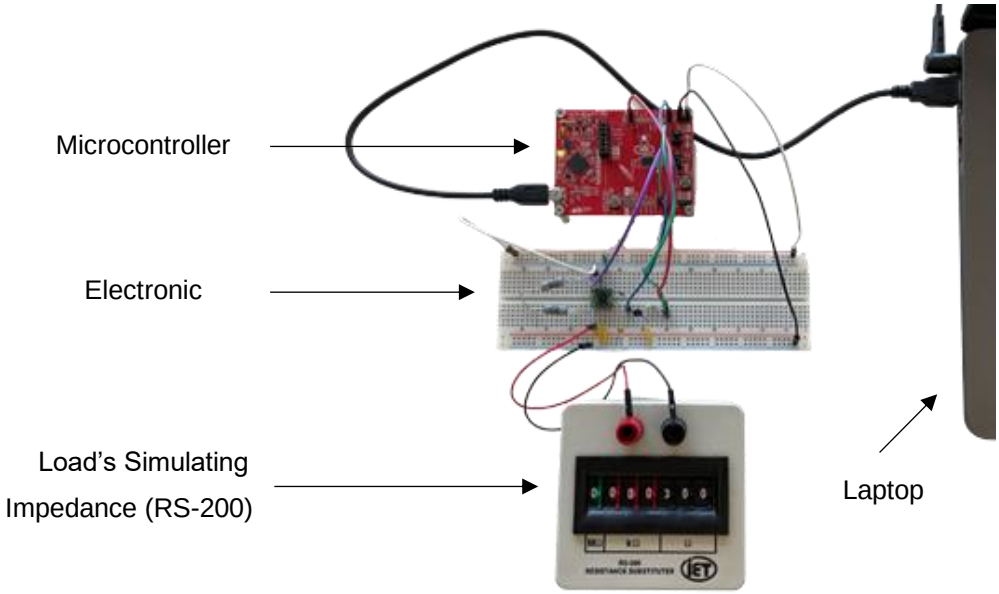

Figure 3.1.7 - Purposed method's simulating circuit.

Compared with the Coulomb counting method, this approach does not need an ADC and high frequency sampling processing is not necessary. Since ADCs usually require high energy consumption comparing to the other Coulomb circuit's components, maintaining the accuracy of this technique, the project's approach will require less power from the device's battery. Subsequently, for spikes with pulses lower than the integrator's period, this circuit avoids losing signal voltage information by not requiring high sampling frequencies since some spikes that may occur during transfers are integrated by the low-pass filter. The goal of the project's implemented approach is to exhibit the correct functioning of this architecture since the integrator outcome resembles an analog-to-digital converter (ADC).

3.2 Microcontroller

3.2.1 Hardware

The MSP430FR2311 was chosen for this project because it has an enhanced comparator (eCOMP) with an integrated 6-bit digital-to-analog converter (DAC) as reference voltage, a low-power ferroelectric RAM (FRAM) and an enhanced USCI A (eUSCI_A) that supports the used UART serial communication. The microcontroller evaluation board is a development kit that helps the coder to test all its functions more easily before the final deployment of the microcontroller to a printed circuit board (PCB). Although very similar compared to other MSP430FR chips, the choice between these microcontrollers was based on the lower standby/shutdown energy consumption, for having all the required functions, and for being in stock for the time being.

3.2.2 Software

In this section, it is made a detailed description of the software in the microcontroller as well as all its processing functions that accomplish all the desires for the project's goal.

The comparator is one of the most important components of the circuit being one of the key reasons why MSP430FR2311 was chosen since not all microcontrollers have this internal comparator. Firstly, the comparator's input pin is connected to the resistor that connects the amplifier's output to the capacitor's anode and the transistor's collector pins, illustrated in Figure 3.2.1.

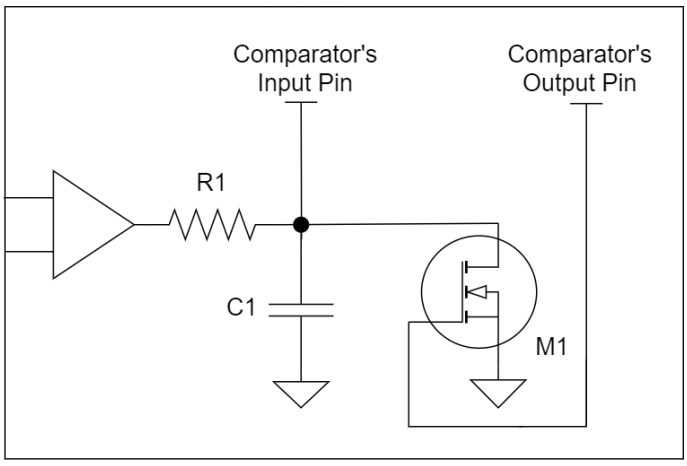

Figure 3.2.1 - Comparator's input and output pins.

Then, in the code, it is used a DAC buffer that states the voltage comparison value on the other comparator's input pin. The comparator's reference voltage and the integrator's impedance and capacity's values were chosen in way that the relationship between the oscillating frequency and the current was as linear as possible and where the current values were more easily distinguished. For this matter, it was chosen a 1 V as the comparator's DAC reference, a 100 kΩ impedance and 330 nF capacitance.

If the capacitor voltage is lower than this value, the comparator output is LOW causing the transistor not to discharge the capacitor and the interruption stays disengaged. On the other hand, if the values are higher than the comparison voltage, as soon as it activates the port, the transistor starts to conduct, the integrator discharges and the comparator's output goes back to zero.

An interruption is needed so that the value of the timer's variable can be retained and reset for calculating the duration between the impulses. Thus, an interruption is activated whenever the output of the comparator goes through a rising flank edge of the comparator's output, the interruption is activated and define the duration between impulses.

For the data transfers between the computer and the MSP430FR2311 microcontroller, it was used a UART communication that performs character by character transmission. After initializing the transmission and reception variables, according to the information obtained by the clock counters, the information of the remaining variables that will be printed are changed. The string is reset by changing each character with the desired numerical value. To print the previously defined string, each character is printed until it reaches the end of the string.

3.3 Coulomb Counting

3.3.1 Hardware

The value of the current measurement should not depend on the sense resistor so that the voltage drop on this resistor is as minimal as possible without compromising the accuracy of this measurement. That said, the maximum voltage drop of the sense resistor should not exceed 1% of the total battery voltage. Worst case scenario, since the sense resistor chosen has an impedance equal to 270 mΩ, the load's equivalent impedance shall be more than one hundred times superior, this is, it must be higher than 27 Ω. Bellow this value, the accuracy of this measurement will fall because the voltage drop on the sense resistor rises.

As explained in the section 3.1, the Op-Amp outputs a range of 1.65 V to 3.3 V voltages for positive inputs since one of the reference voltages are connected to ground and the other to the Microcontroller's Vref. Thus, the output of the Op-Amp is calculated by summing the 1.65 V to twenty times the value of the sense resistor's voltage, Vs,

$$\mathrm{Vop\ (V)} = 1.65 + 20 \times \mathrm{Vs}. \tag{15}$$

Therefore, the maximum input voltage of the Op-Amp is,

$$\mathrm{Vs_{MAX}\ (mV)} = \frac{3.3 - 1.65}{20} = 82.5\ \mathrm{mV}. \tag{16}$$

It is possible to calculate the maximum current that can be measured by dividing the maximum amplifiable input voltage with the impedance of the sense resistor,

$$\mathrm{I_{MAX}(mA)} = \frac{82.5\ \mathrm{mV}}{270\ \mathrm{m\Omega}} \cong 306\ \mathrm{mA}. \tag{17}$$

With a 3 V battery and for the situation of 1% voltage drop on the sense resistor, the maximum current value that this project can measure is,

$$\mathrm{I} = \frac{3\ \mathrm{V}}{27\ \Omega + 270\ \mathrm{m\Omega}} = 110\ \mathrm{mA}. \tag{18}$$

For the 9 V battery and with 1% voltage drop, the maximum current is,

$$\mathrm{I} = \frac{9\ \mathrm{V}}{27\ \Omega + 270\ \mathrm{m\Omega}} = 330\ \mathrm{mA}. \tag{19}$$

Which is higher than the maximum current calculated in (17) that corresponds to the milliamperage value of the maximum amplifiable voltage. Hence, for general use, the maximum current measurement for this project was limited to 110 mA.

Known as “RS-200 Decade Box” and illustrated in Figure 3.3.1, the sense resistor was connected to this device that simulates to a load’s constant impedance.

Figure 3.3.1 - RS-200 decade box.

The RS-200 decade box is a portable device that is convenient for simulations where the tests don’t require periodic changes on the resistor’s impedance value. Further on, it will be needed a resistor capable of changing its value to maintain a constant current for the device since the battery’s voltage decreases with use. Therefore, it was used a “Programmable Resistance Substitute”, illustrated in Figure 3.3.2, that connects to the laptop and communicates with the LabView program. Whenever the voltage acquired with the DAQ changes its value, the system programs the resistor to maintain the desired current.

Figure 3.3.2 - PRS Series Programmable Resistance Substituter.

As stated in the section 3.1, since the pulses are caused by comparing the signal from the capacitor to the voltage of 1 V during the charging of this component, the greater the Op-Amps output voltage, the greater the current that passes through the capacitor and, consequently, the faster it charges. Because the Op-Amp’s output is between the range of 1.65 and 3.3 Volts, the signal is continuously being integrated and, consequently, there is always a minimum and maximum range of pulses per second. The Table 3.3.1 shows the range of the oscillating frequency (number of pulses per second), duration between pulses, and the corresponding Op-Amp’s output voltages.

Table 3.3.1 - Voltage, frequencies, and duration between pulses for different currents.

Discharged Current (mA)	Op-Amp Output Voltage (V)	Oscillating Frequency (Hz)	Duration Between Pulses (ms)
306	3.3	87	11.5
110	2.25	54	18.5
1	1.66	34	29.4

The duration between pulses is measured with the microcontroller's timer function where it is continuously counting. When the comparator's output is HIGH, the interrupt is enabled, the timer's value is stored and then reset. The time between these pulses is inversely proportional to the current supplied by the battery, this is, the greater the measured current, the lower the duration between pulses. On the other hand, the capacitor's maximum charging time occurs when the Op-amp is saturated, in other words, when the current is at its minimum measurement value.

Raising the value of the capacitor makes it have more charge capacity and consequently takes longer to charge it. Increasing the value of the integration resistance makes the current smaller and consequently takes longer to charge the capacitor. Thus, increasing the resistance-capacitor (RC) integrator lowers the charging and discharging frequency and vice versa. Therefore, the RC dimensioning is important as it defines the energy consumption for the integration effect as well as for setting the sampling frequency. The discharging current is fully integrated and all the charge that was discharged from the battery is measured since it has a high sampling frequency from charging and discharging the capacitor. The lower the capacitor's value, the higher the sampling frequency but the lower the precision of the current measurement because the integration time is reduced.

3.3.2 Software

In this section it is explained how the SOC is estimated in software by using some formulas that relate the time measured for each HIGH comparator output pulse with the discharged current. Firstly, the time is measured by setting and resetting the timer for each pulse. This measurement is the time the capacitor takes to reach the comparison value of 1 volt calculated by,

$$t_{PW} = -RC \times \ln\left(\frac{1}{V_f}\right). \quad (20)$$

Where RC is a multiplication of the resistor and capacitor responsible for the current integration. Then, since V_f is the output voltage of the Op-amp, the voltage of the sense resistor is calculated by,

$$V_f = V_{offset} + G \times U_{sense}. \quad (21)$$

Where V_{offset} is the offset voltage of 1.65 V and G is the gain of the Op-amp. Knowing the U_{sense} voltage value, the discharge current is the ratio of this voltage by the sense resistor's impedance,

$$I_d = \frac{U_{sense}}{R_{sense}}. \quad (22)$$

The electric charge (C) may be calculated with the multiplication of the time between pulses, t_{PW}, with the value of the discharged current,

$$\mathrm{C\ (mAh)} = \mathrm{I_d} \times \mathrm{t_{PW}}. \tag{23}$$

The discharged current is calculated with (24) where the constant V_0 is the comparing voltage which is equal to 1 V and RC is the multiplication of the resistor with the capacitor's values.

$$\mathrm{I_d\ (mA)} = \frac{\mathrm{V_0(V)}}{\mathrm{R(\Omega)}} \times \mathrm{e}^{-\mathrm{t_{PW}}/\mathrm{RC}}. \tag{24}$$

The percentage drop per sample (PDS) is calculated by diving the capacity of the battery in seconds (mAh/3600) by the electric charge,

$$\mathrm{PDS\ (\%)} = \frac{\mathrm{C\ (mAh)}}{\mathrm{Battery\ Capacity\ (mAh)}} \times \frac{1}{3600} \times 100\%. \tag{25}$$

The PDS is dependent on the battery capacity as well as the capacity on the type of battery used. Therefore, several look-up tables are made dependent on the three alkaline and two lithium-iron disulfide types of batteries. Since for 1 mA to 110 mA current range, only the battery capacity of the alkaline cells varies on the discharge current, three look-up tables were made for the alkaline AAA, AA and 9-Volt and just one for AAA and AA lithium batteries. The PDS look-up table is calculated and exported to the microcontroller with the corresponding pulse-width values. Starting at 100%, the SOC of charge is estimated by subtracting it by the PDS using look-up tables with interpolation,

$$\mathrm{SOC_n\ (\%)} = \mathrm{SOC_{n-1}(\%)} - \mathrm{PDS_{Average}(\%)}. \tag{26}$$

The time measured by microcontroller is compared to the two most approximated values of the table and PDS is calculated by this linear interpolation. Then, the SOC value is printed alongside the timer for posterior graphic illustrations.

3.4 Production Cost

A detailed cost for each component used for the project is presented in Table 3.4.1 to demonstrate its low-cost production. Of course, this number is an illustrative cost that in a real situation some components could be spared depending on the system used. The price presented is the lowest offered value between some companies that sell these electronic components.

Table 3.4.1 - Overall production cost of the project.

Component	Reference	Quantity	Store	Unitary Price (€)	Price (€)
Processor	MSP430FR2311	1	Mouser	1.56	1.56
Capacitors	-	10	Mauser	0.21	2.10
Resistors	-	2	Mouser	0.415	0.83
Transistor	BS170	1	Electrofun	0.75	0.75
Op-amp	AD8418WBRZ	1	Mouser	2.71	2.71
PCB	-	1	Electrofun	2.09	2.09
				Total:	10.04

3.5 User Interface

In this sub-section, a description and illustration of the user interface (UI) is made. This UI was developed in LabView, and it allows a cleaner and easier way for the communication between the user and the processor. The Figure 3.5.1 shows the designed layout of the user interface in the “CCS SOC” tab, the project’s Coulomb Counting data, composed by:

- Three buttons: “Update” initiates the program and updates manually if pressed during the acquisition; “Stop” interrupts the program by setting the processor to sleep and saving the acquisition data in a “.mat” file for MATLAB posterior analysis; and “Restart” reinitializes the values of the “Clock”, “Samples” and battery’s SOC.
- Three numerical controls: “Open Circuit Voltage (V)” and “Discharge Voltage (V)” are the voltage values and to characterize the batteries; “Auto Update (s)” for the seconds between each acquisition; “Timer (h)” is the number of hours, and “Timer (min)” is the number of minutes the user wants the program to run; and “Current (mA)” is the desired constant current for the system to program the resistor as the voltage decreases its value.
- Four different data displays: “Clock” shows the time the program has been running; The SOC is displayed bellow the battery icon; “Samples” is the number of acquisitions made; “Pulse Width (µs)” is the time between impulses; “Current CCS” is the measured current; and “Acquisition Progress (%)” is the ratio between the “Clock” and “Timer” values displaying the progress of the program in percentage.
- A battery SOC graph indicating the battery’s percentage with the acquisition time in seconds.

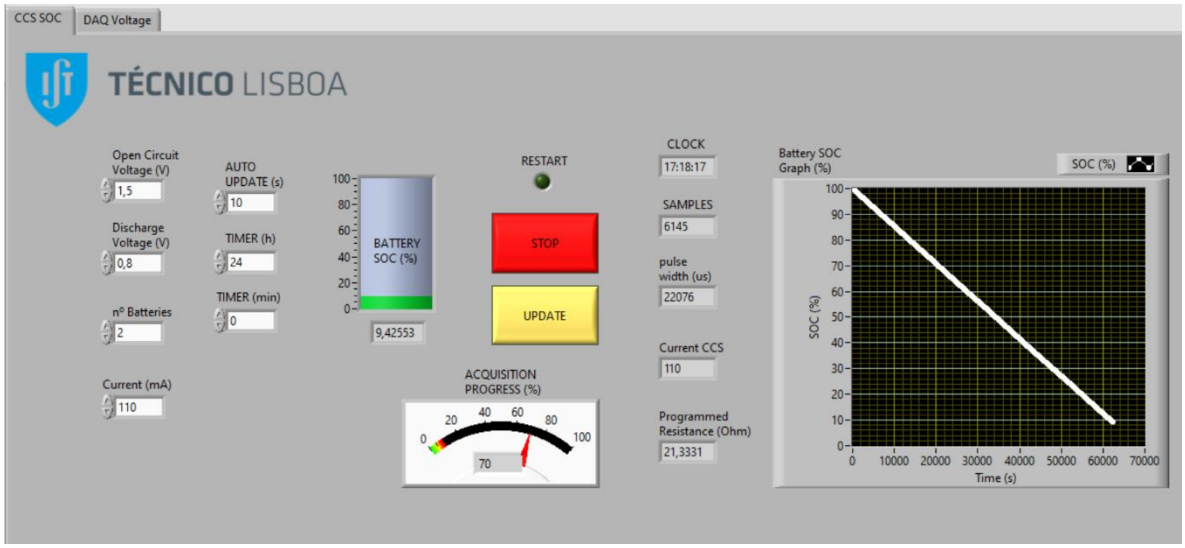

Figure 3.5.1 - LabView UI "CCS SOC" tab.

In this case, the figure illustrates an acquisition of two AA lithium iron disulfide Energizer batteries being made for about five hours with ten seconds between each acquired sample, the battery’s SOC is 9.4% and the program is at 70% of its twenty-four hours acquisition time.

The Figure 3.5.2 shows the designed layout of the user interface in the “DAQ” tab composed by:

- An “Update” button that starts the program and updates manually if pressed during the acquisition.
- “Samples” data displays the number of acquisitions made.
- A Voltage graph indicating the battery’s nominal voltage with the acquisition time in seconds.

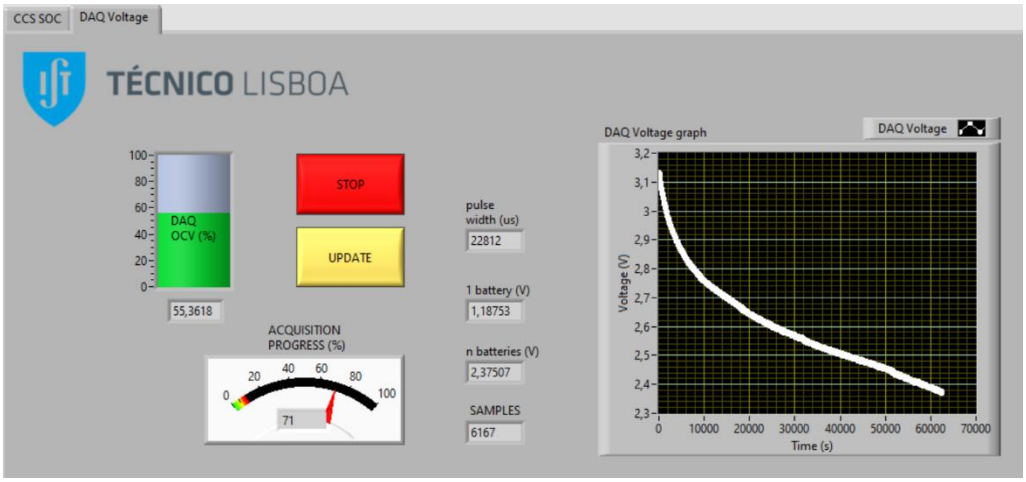

Figure 3.5.2 - LabView UI "DAQ" tab.

In this case, for the seventeen hours of acquisition and two AA cells of 1.5 V, the OCV is expected to lower its value to approximately 1.6 V equivalent to twice the discharge voltage of an AA alkaline battery. When it reaches this value, it is considered as a “dead” battery no longer capable of delivering the intended charge. This OCV graph can be predicted and is posteriorly compared with the battery’s corresponding voltage graph presented in its manufacturer’s datasheet of the corresponding battery.

3.6 Battery Capacity Estimations

In this section it will be demonstrated how the battery's capacity was estimated depending on its discharging current for the three different alkaline battery types. Since the charge capacity of lithium batteries don't depend on the discharging current in the project's current measurement range, these functions were only destined to the three types of alkaline batteries: AAA; AA; and 9 V.

The Figure 3.6.1 is the chart presented in the AAA alkaline battery manufacturer's datasheet that illustrates the battery capacity depending on the continuous discharge to 0.8 V at 21ºC [23].

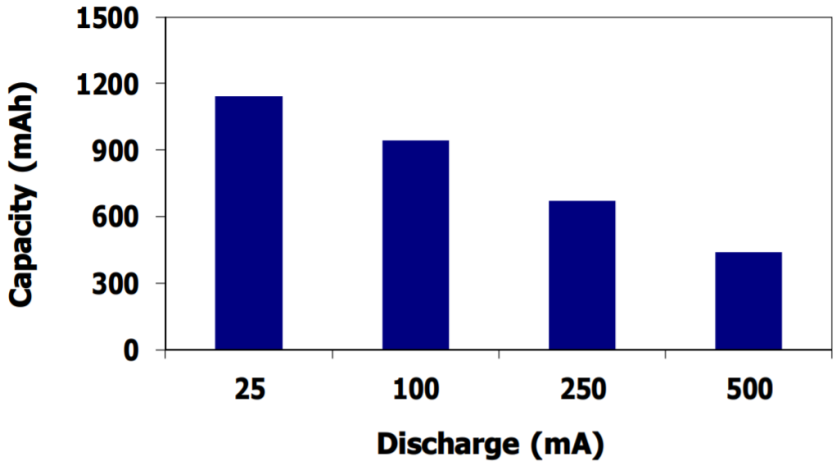

Figure 3.6.1 - AAA alkaline Energizer battery capacity with discharge current [23].

Demonstrated in Figure 3.6.2, it was made a function that estimates the capacity of the AAA battery depending on the discharge current.

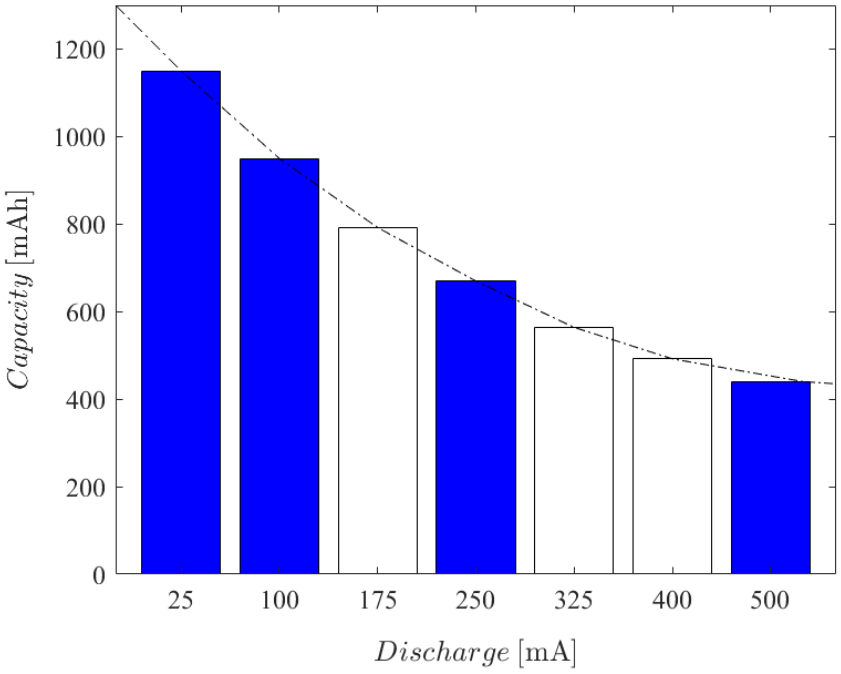

Figure 3.6.2 - AAA battery capacity estimation function.

The estimated function of the AAA alkaline battery's capacity, f_{AAA}, represented dashed line and afterwards directly related to the discharge current in the microcontroller, is dependent on the discharge current, I_d, and on the nominal capacity of the battery, C_n,

$$f_{AAA}\,(\mathrm{mAh}) = \frac{(I_d)^2}{400}(\mathrm{mAh}) - 2.77 \times I_d(\mathrm{mAh}) + C_n\,(\mathrm{mAh}). \tag{27}$$

For the AA alkaline batteries, the chart of the Figure 3.6.3 shows the approximate capacity depending on the discharged current to 0.8 V at room temperature [25].

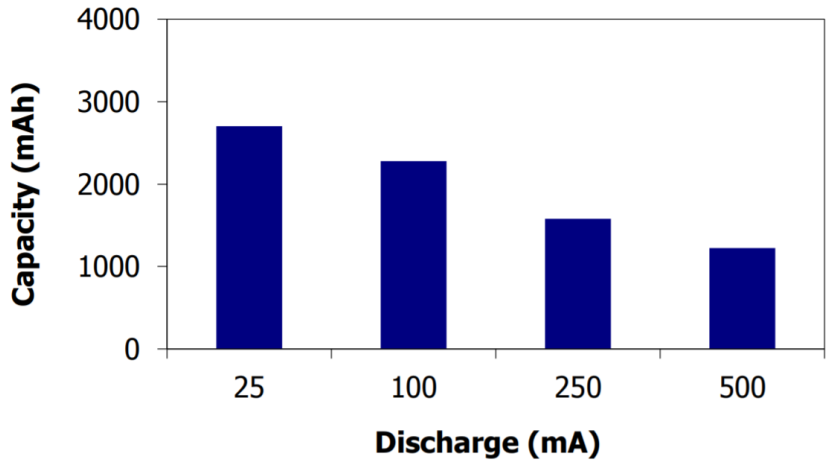

Figure 3.6.3 - AA alkaline Energizer battery capacity with discharge current [25].

To estimate the battery capacity of these batteries, in the same way as the AAA batteries, the Figure 3.6.4 illustrates the function made that approximated the charge capacity values depending on the current being discharged.

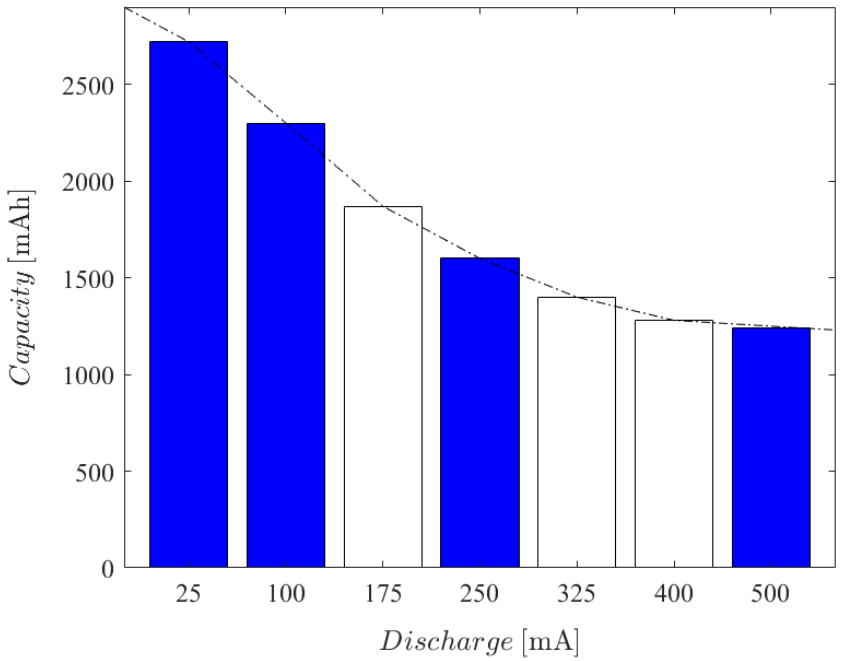

Figure 3.6.4 - AA battery capacity estimation function.

The estimated function represented in the dashed line is the function for the AA battery's capacity, f_{AA}, and posteriorly related to the discharge current in the microcontroller,

$$f_{AA}\,(\mathrm{mAh}) = \frac{(I_d)^2}{137} - 7 \times I_d + C_n\,(\mathrm{mAh}). \tag{28}$$

Lastly, the Figure 3.6.5 is a chart from the datasheet of the 9V battery's manufacturer that shows its approximate capacity depending on the current being discharged [26].

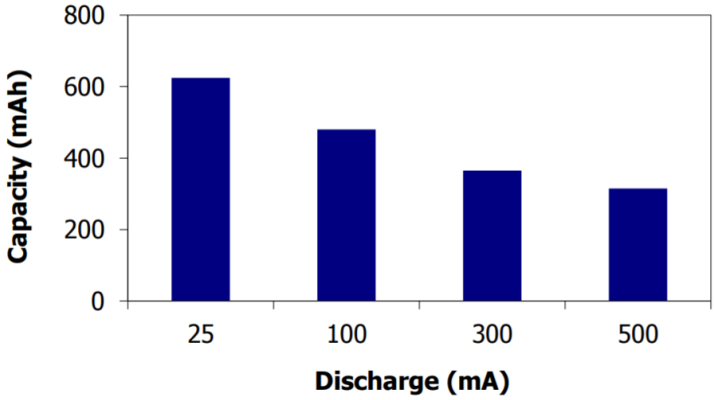

Figure 3.6.5 - 9 V alkaline Energizer battery capacity with discharge current [26].

Illustrated in Figure 3.6.6, an approximation of the graph was made to have an estimation on the battery capacity with the discharge current.

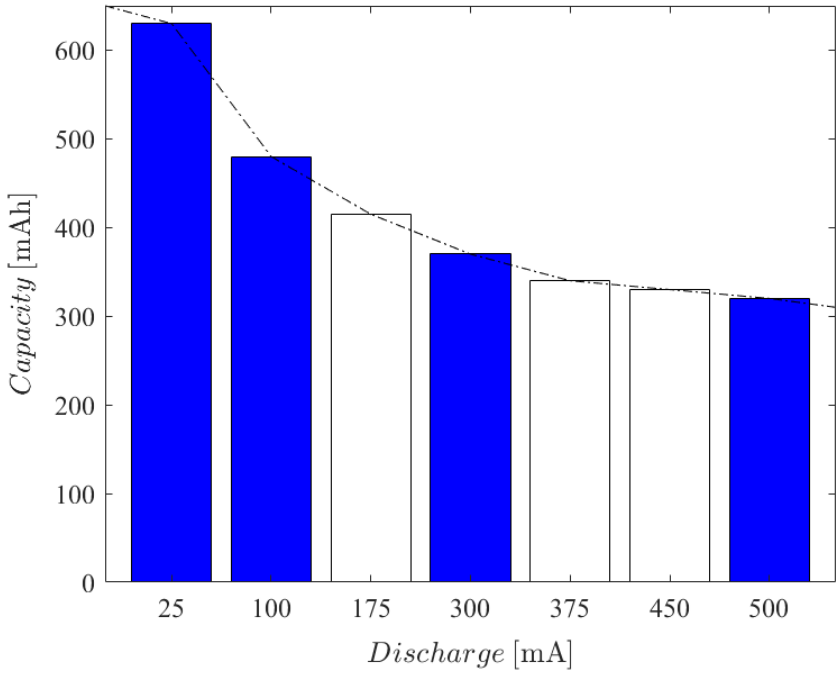

Figure 3.6.6 – 9 V battery capacity estimation function.

The dashed line is the estimated function of the 9 V battery's capacity, f_{9V}, and afterwards directly related to the discharge current in the microcontroller,

$$f_{9V}\,(\mathrm{mAh}) = \frac{(I_d)^2}{476} - 1.7 \times I_d + C_n(\mathrm{mAh}). \tag{29}$$

4. Experimental Results

Experimental Results

4.1 Characterization Results

In this section, all the project's intended measurements and designed ranges for the characterization results are addressed. As stated in section 3.3.1, this project is designed to work for current measures between 1 mA and 110 mA for better precise and accurate measurements. Illustrated in Figure 4.1.1, the time between pulses varies logarithmically with the current. The shorter the duration between these pulses, the higher the current and vice-versa. Thus, the green line in Figure 4.1.1 is a trendline of the most accurate measuring range since they are measurements beyond the vertical and horizontal asymptotes of this function and for being the range for less power consumed by the sense resistor.

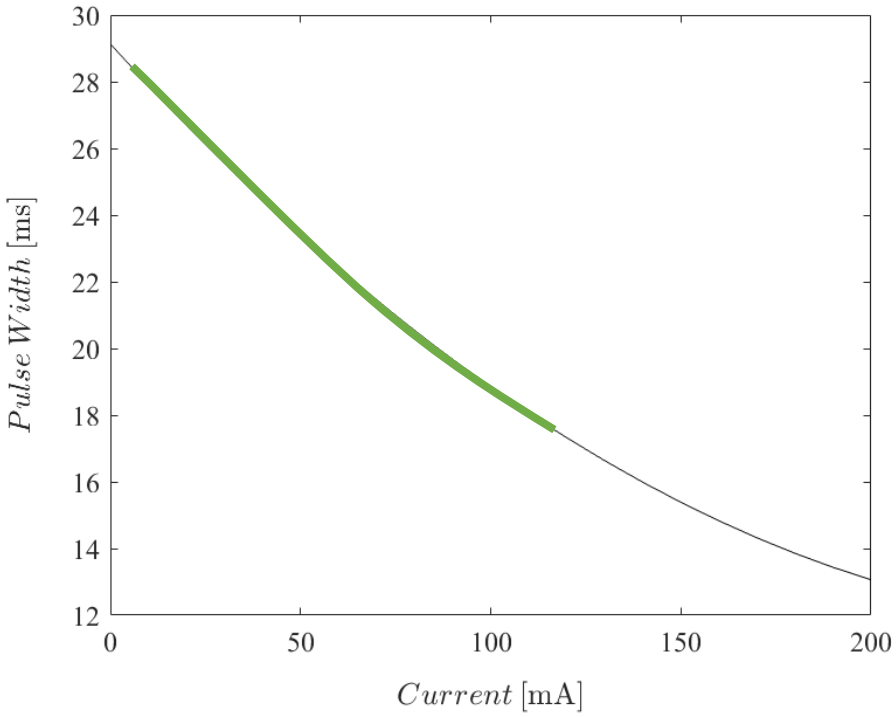

Figure 4.1.1 - Plot of duration between pulses and corresponding current.

Only batteries with the compound of alkaline and lithium iron disulfide were tested since they are both commonly seen in IoT devices, non-rechargeable and, consequently, comparable. Although these batteries have different chemicals, they share the same shapes and sizes of AA and AAA batteries. The rectangular shaped 9 V batteries are only manufactured with the alkaline compound and are commonly used in IoT devices. Therefore, for this project, five different types of batteries were tested: AA and AAA lithium; and AA, AAA and 9V alkaline batteries.

Measurement errors come from the time it takes the MSP to perform its functions, possible rounding, temperature, equipment errors, datasheet approximations and even the errors that each battery employs described by its manufacturer. These measurements were made with Energizer batteries since the performance, capacity, current dependency, temperature, technology, and materials are easily comparable between the different types of batteries.

The battery's percentage drop per acquired sample (PDS) depends on the battery capacity as stated in section 2.6 and in section 3.6 it was illustrated the battery capacity estimation functions made that include this current dependency. As illustrated in Figure 4.1.2, the blue line represents the test made on two 1.5 V alkaline batteries with different discharging currents every hour and the orange line the theorical battery capacity without current dependency.

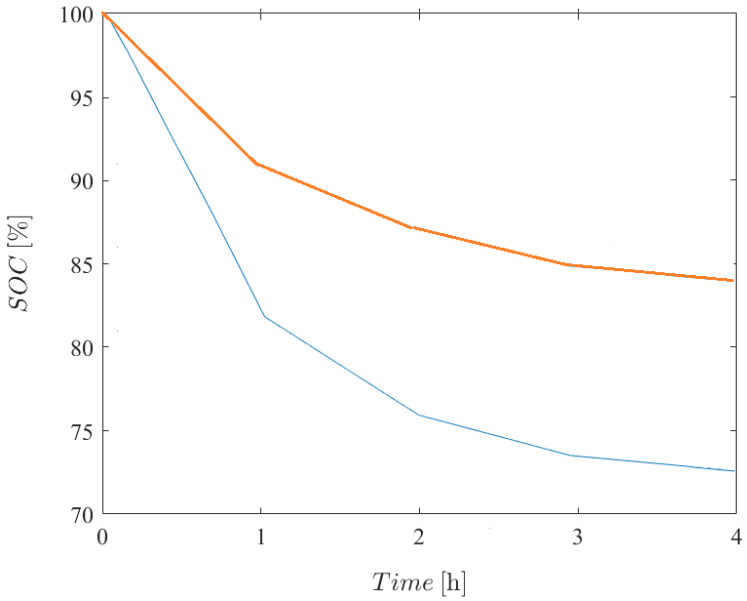

Figure 4.1.2 – Varying the discharging current every one hour.

In this test, from 100% to about 83%, the battery is discharging 100 mA and consequently discharging a total of 17% of the nominal capacity per hour. Then, in the second hour of the test, the battery drops from 83% to 76% with 50 mA, posteriorly from 76% to 74% with 25 mA and lastly from 74% to 73% with 10 mA of discharging current. In the Table 4.1.1, the values of the blue and orange dots are presented to emphasize the importance of knowing the battery's dependence on the current to be discharged.

Table 4.1.1 - Values of the battery's SOC with and without current dependency.

Discharge Current (mA)	Drop per hour with current dependency (%)	Drop per hour without current dependency (%)
100	17.46	8.34
50	5.79	4.19
25	2.42	2.10
10	0.84	0.84

Although very precise, these results are still approximations from data token from the batteries' datasheets that, as stated, are presented as a reference of physical values that were not intended for specific calculations [22]. Since the function of the battery capacity approximations is dependent on values from tests performed at room temperature, the error is higher outside the range of 20ºC to 22ºC.

4.2 Expected Results

For comparison and validation, two methods were made to verify the SOC measured by the circuit: voltage and capacity discharge comparisons. The first method, SOC_1, was to acquire the voltage of the DAQ measurement, V_{DAQ}, with the range of the battery's nominal voltage, Vn, and discharged voltage, Vd. The voltage of a battery decreases with use, and the sourced circuit won't work properly bellow the discharged voltage stated in the manufacture's datasheet. Therefore, the nominal voltage is set as the 100% battery's SOC reference and the discharged voltage as the 0% empty charge,

$$\mathrm{SOC_1}\ (\%) = \frac{(\mathrm{V_{DAQ}} - \mathrm{V_d})\ (\mathrm{V})}{(\mathrm{V_n} - \mathrm{V_d}\ )\ (\mathrm{V})}. \tag{30}$$

The main drawback of this method is for not being precise since the battery's voltage decreases more when reaching the discharged voltage value than between these two references. In that matter, the second method, SOC_2, takes place by calculating the ratio of the discharged capacity from the battery, Cd, and the nominal capacity, Cn, stated by its manufacturer,

$$\mathrm{SOC}_{\ 2}\ (\%) = \frac{\mathrm{C_d}\ (\mathrm{mAh})}{\mathrm{C_n}\ (\mathrm{mAh})}. \tag{31}$$

Although being precise, this method won't work if the discharged current is unknown, or it wasn't constant in all the acquisition time since the discharged capacity can only be calculated knowing the discharged current, I_d and the acquisition time t_a,

$$\mathrm{C_d}\ (\mathrm{mAh}) = \mathrm{I_d}\ (\mathrm{mA}) \times \mathrm{t_a}\ (\mathrm{h}). \tag{32}$$

During acquisitions, the value of the discharge current varied as the voltage of the battery varies with use. However, as the initial and final current values can be known by calculating the ratio of the battery's voltage with the known constant impedance, the current used can be estimated and, consequently, the capacity that has been removed from the battery is determined,

$$\mathrm{I_d}\ (\mathrm{mA}) = \frac{\mathrm{V_{DAQ}}\ (\mathrm{mV})}{\mathrm{R}\ (\Omega)}. \tag{33}$$

The results are expected to vary depending on the current discharged from the battery and the type used: alkaline or lithium. The nominal capacity of alkaline batteries varies depending on the discharged current, however, as stated in section 2.6, the capacity does not vary for lithium batteries in the limited measuring range of this project.

From the nominal voltage, V_n, to the discharged voltage, V_d, with the same impedance it is possible to calculate the maximum current, I_{max}, and the minimum current, I_{min}.

Measured with the DAQ device, the voltage of the AA and AAA alkaline batteries is expected to start around 10% above the nominal value and go down to around 60% below the nominal voltage value, representing the battery's offset and discharge voltage, respectively, identically to the graph represented in Figure 4.2.1 [25].

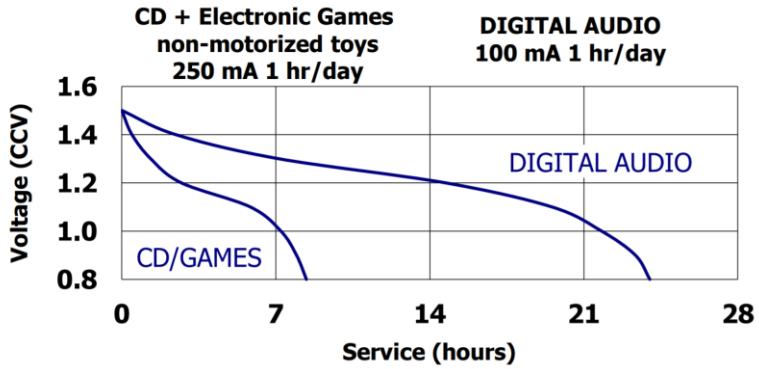

Figure 4.2.1 - OCV voltage within AA Energizer alkaline battery's service hours

As for lithium iron disulfide AA and AAA batteries, the voltage is linear from its nominal value 1.5 V to 1.2 V and then peaking down to its discharge voltage of 0.8 V, illustrated in Figure 4.2.2. Therefore, the current does not vary its value as much as the alkaline cells with a constant impedance.

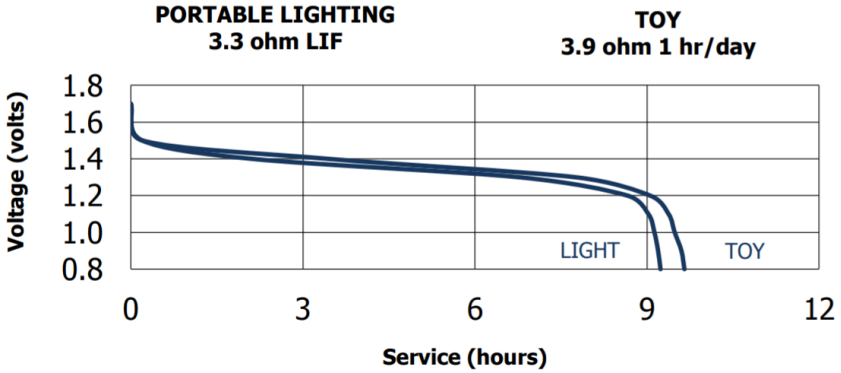

Figure 4.2.2 - OCV voltage within AA Energizer lithium iron disulfide battery's service hours

On the other hand, for the Energizer 9 V batteries, the initial voltage is expected to be equal to 9 V and to drop to its discharge voltage of approximately 4.8 V. As shown in Figure 4.2.3 of the Energizer 9 V battery datasheet, since the voltage represented is in OCV, the rated voltage of the project's measurement in closed circuit is expected to be lower [26].

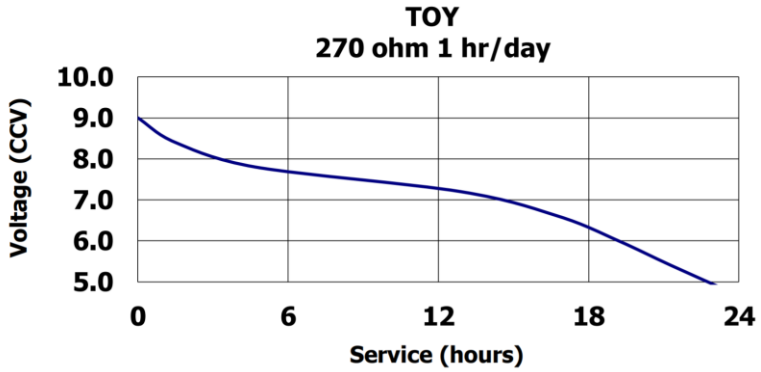

Figure 4.2.3 - OCV voltage within 9 V Energizer battery's service hours [26].

In the second method, since the tests performed on the batteries were carried out with a constant load impedance, as the battery voltage decreases, the current also decreases and the time for the battery's complete discharge increases. Therefore, it was made a linearization of the voltage with the discharge time and the average current was calculated. With a constant load impedance, R, the way to

predict the time for a battery to fully discharge, t_d, is the ratio of the battery's nominal capacity with the average discharge current, I_d,

$$t_d\ (\mathrm{h}) = \frac{C_n\ (\mathrm{mAh})}{I_d\ (\mathrm{mA})}. \tag{34}$$

The graph of SOC with time is expected to be linear until the battery reaches approximately 70% of the nominal voltage where the discharge current is expected to decrease logarithmically. These calculations are important because they help to predict the behavior of the battery to prove the results obtained through the proposed method of the Coulomb integrator.

To improve the second method's measurements, a programmable variable resistor was used to obtain a constant current. The graph of the SOC with this improvement will be entirely linear throughout all acquisition time and, consequently, the battery discharges faster.

4.3 Validation Results

The data acquired from the microcontroller and the DAQ device were gathered and graphically displayed for validation of the project's measurements. The goal is to compare alkaline and lithium iron disulfide batteries' behaviors exposed to different operational temperatures or to high discharging currents. To validate these results, the graphs were compared to the datasheet of the batteries' manufacturer and to the voltage measurement acquired with the DAQ device.

4.3.1 AAA Batteries

In this section, the acquired results from the tests made on alkaline and lithium iron disulfide AA and AAA batteries as on the 9 V alkaline rectangular battery will be presented. Between each test, the results obtained are compared with the expected ones detailed in the previous section 4.2.

Although AAA, AA and 9 V alkaline batteries have an approximate capacity of 1200 mAh, 2900 mAh and 650 mAh, respectively, the nominal capacity of these batteries varies significantly depending on the discharge current. Comparing Energizer's AAA, AA, and 9 V alkaline batteries, AA batteries are more dependent on the discharge current than AAA and the 9 V batteries are less on the required current than AAA. Based on the datasheet provided by the manufacturer of these batteries, functions were made to adjust the values of the nominal capacities of the batteries according to the discharged current.

The first test was performed with two 1.5 V AAA batteries in series supplying a constant 27 Ω impedance. Using two batteries in series instead of just one, the voltage doubles and, consequently, the current doubles, but the capacity of the two batteries remains the same. With a constant impedance of 27 Ω, the initial current is approximately equal to 110 mA and the final current is approximately equal to 66 mA. According with the manufacturer's datasheet, the expected capacity of these batteries for the current range of this test should be approximately equal to 930 mAh instead of the 1200 mAh nominal capacity. The graph illustrated in Figure 4.3.1 of the battery's voltage over the capacity drained was obtained with a constant 27 Ω resistance.

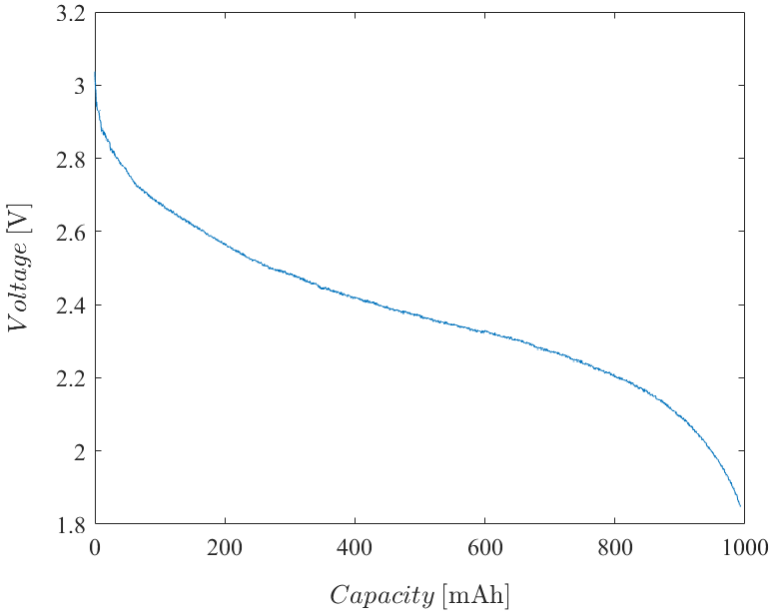

Figure 4.3.1 - Voltage and drained capacity of two AAA alkaline Energizer batteries with 27 Ω load impedance (21ºC).

As expected and explained in section 4.2 of the expected results, since the voltage decreases over time of use, the current also decreases its value. To counteract this effect, it is necessary to use the programmable resistor device explained in section 3.3.1. This device allows the program to choose the impedance value according to the voltage of the batteries so that it is possible to discharge the batteries with a constant current. Thus, a second test was carried out with batteries equal to the first acquisition. Illustrated in Figure 4.3.2, the graph of the SOC and voltage of the batteries over the acquisition time with a constant 110 mA current was obtained.

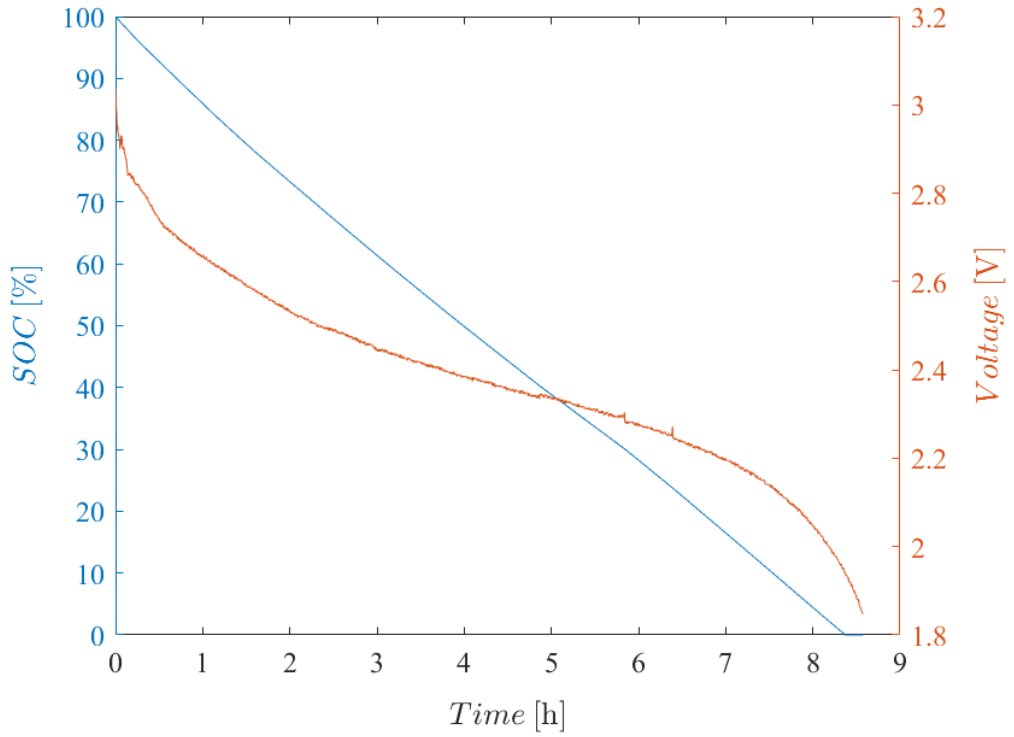

Figure 4.3.2 - SOC and voltage of two AAA alkaline Energizer batteries with 110 mA discharge current (21ºC).

Comparing the Figure 4.3.1 with Figure 4.3.2, it is possible to see the various sorts of behaviors of these types of batteries. First, the voltage decreases cubically and naturally with its use, proving the natural performance of a battery explained in section 2.1. Consequently, the first test done with constant resistance, the current was decreasing leading the SOC to lower its value with a greater slope until reaching a certain time at which the slope decreases. After approximately eleven hours, the batteries reached 1.8 V, which represents twice the discharge voltage of an Energizer AAA battery, and they stop working normally. In the graph of the constant impedance, knowing that the current decreases as the voltage decreases, the battery capacity increases as the current value decreases. Given that the average battery capacity of this first test is approximately equal to 976 mAh and that the current goes down with the acquisition time, the test took approximately eleven hours.

In the second graph, the batteries took less time to discharge. With a capacity of 1200 mAh and a discharge current of 110 mA, without current dependency, theoretically the battery should last eleven hours, t_{th}, until full discharge,

$$t_{th}\,(\mathrm{h}) = \frac{1200\ \mathrm{mAh}}{110\ \mathrm{mA}} = 11\mathrm{h}. \tag{35}$$

Due to the dependence on these two variables, the batteries lasted less than nine hours with constant current and, consequently, the discharge capacity of these batteries on this test was,

$$C_d = 110\ \mathrm{mA} \times 8.4\ \mathrm{h} = 924\ \mathrm{mAh}. \tag{36}$$

Differently from the first test, the second graph of the constant current took less time to drain the batteries since the expected capacity for this current is smaller and the discharge current as higher value than the average values of the first test.

Although AAA lithium iron disulfide have just over 100 mAh more than the nominal capacity of the AAA alkaline batteries, the big differences between these two types of batteries are on not depending on the discharge currents bellow 1 A and not having operating anomalies when working on temperatures in the range of 0ºC and 60ºC. Since the project was design to measure currents between the range of 1 mA and 110 mA, the capacity of lithium iron disulfide cells does not depend on the discharged current. Comparing Energizer's AAA and AA, the only differences between these two are weight, size, and battery capacities. In Figure 4.3.3 it is presented the voltage and capacity drained of the first test carried out with two 1.5 V AAA lithium batteries with a 27 Ω of the load's impedance and consequently 110 mA of initial current.

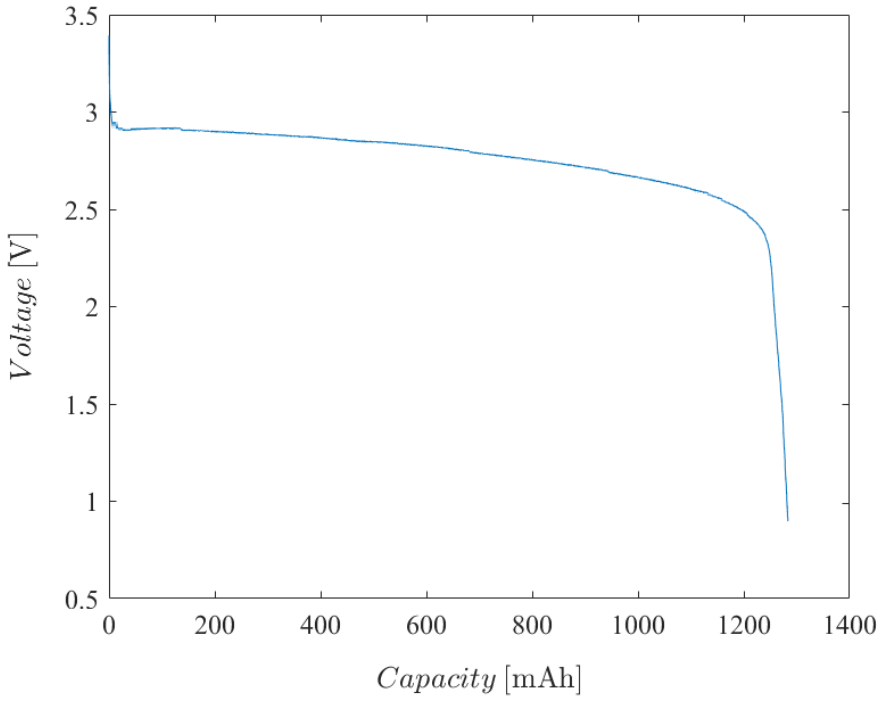

Figure 4.3.3 - Voltage and drained capacity of two AAA lithium Energizer batteries with 27 Ω load impedance (21ºC).

Since the voltage of these two batteries varies cubically between the nominal 3 V and 2.4 V, respectively, the current varies cubically too from 110 mA to 88 mA, with the average discharge current, I_d, being around 100 mA. Differently from the alkaline batteries, on these lithium iron disulfide batteries, the average discharge current is simply important for knowing the expected time for the batteries to discharge completely,

$$t_a = \frac{1300\ \text{mAh}}{100\ \text{mA}} = 13\ \text{h}. \tag{37}$$

For a device that needs a constant discharge current, the capacity remains the same but the time for a complete discharge is reduced naturally to approximately eleven hours with the increase of the I_d,

$$t_a = \frac{1300\ \text{mAh}}{110\ \text{mA}} \cong 12\ \text{h}. \tag{38}$$

Thus, comparing time results from a constant resistance to the ones from a constant current, the time to discharge the batteries of these two are almost the same since the batteries voltage varies only from the 1.5 nominal voltage to approximately 1.2 V with lithium iron disulfide instead of 0.9 V of the alkaline cells. The SOC and voltage of the batteries in Figure 4.3.4 are a result of the second test's performance with a constant current of 110 mA. As stated in section 2.6.2 and since the batteries took in fact less than twelve hours for a complete discharge, this proves that the capacity of litihum iron disulfide cells don't depend on the discharge current bellow 1 A.

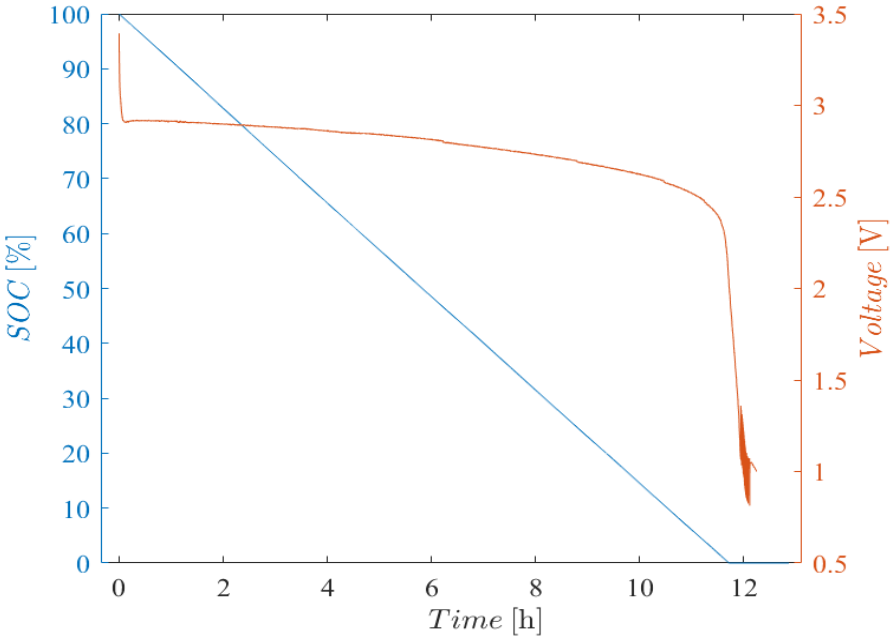

Figure 4.3.4 - SOC and voltage of two AAA lithium Energizer batteries with 110 mA discharge current (21ºC).

4.3.2 AA Batteries

After the acquisitions on AAA alkaline batteries, the AA alkaline batteries were tested and, comparing these two, AA are batteries with the same nominal voltage but with more capacity. In question, the batteries used for these tests from Energizer have around 2900 mAh, almost the triple the amount of charge capacity of the AAA batteries from the same manufacturer. Illustrated in Figure 4.3.5, the first test was performed with a constant resistance of 27 Ω and an initial current of 110 mA.

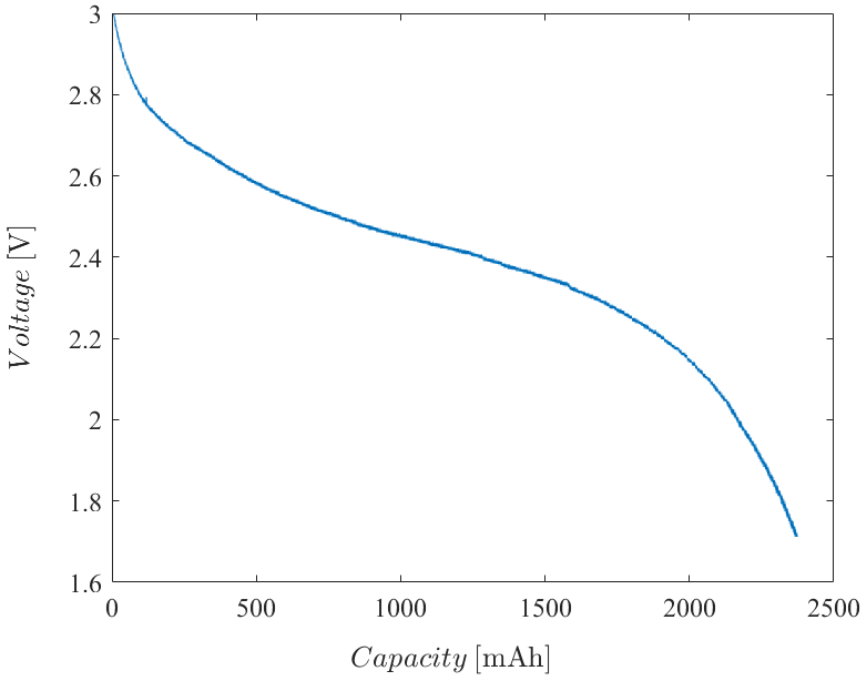

Figure 4.3.5 - Voltage and drained capacity of two AA alkaline Energizer batteries with 27 Ω load impedance (21ºC).

The test took approximately twenty-seven hours for the batteries to reach the discharged voltage announced in the manufacturer's datasheet. Since the average discharge current was approximately equal to 88 mA, the charge received from the battery was,

$$C_d = 88\,\text{mA} \times 27\,\text{h} = 2376\,\text{mAh}. \quad (39)$$

This means that the capacity discharged from the battery was lower than the 2900 mAh nominal capacity proving once again the dependency on the current being discharged from the battery.

However, with dependence on constant discharge current, the capacity is about 23% less, 2220 mAh instead of 2900 mAh, discharging it in approximately twenty hours. Therefore, the test was performed with a constant discharge current, shown in Figure 4.3.6. This test took less time to fully discharge the battery than the estimated theoretical time, consequently proving the battery's charge capacity dependency on the discharge current.

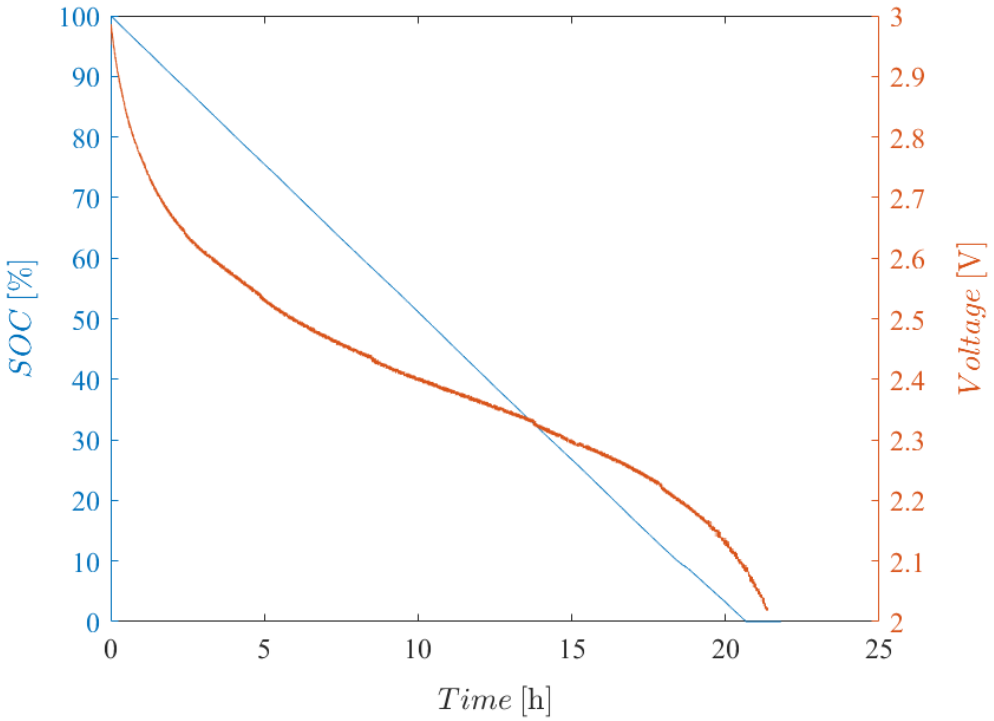

Figure 4.3.6 - SOC and voltage of two AA alkaline Energizer batteries with 110 mA discharge current (21ºC).

The tests were all performed at room temperatures of around 21°C such as the graphs tooken from the manufacturers' datasheets in the expected results of section 4.2.1. For a 110 mA constant current, according to the battery's manufacturer and as estimated in section 3.6, the charge that the battery can deliver is approximately 2200 mAh instead of the nominal 2900 mAh and, as a result, this test took approximately twenty hours,

$$\mathrm{C_d} = 110\ \mathrm{mA} \times 20\ \mathrm{h} = 2200\ \mathrm{mAh}. \tag{40}$$

The SOC blue graph does not drop to 0% at the same time as the orange voltage graph due to possible measurement errors as well as the temperature not being precisely equal to the twenty-one degrees Celsius results from the battery's datasheet.

As mentioned in section 2.6.1, the capacity of the batteries depends not only on the discharge current but also on the temperature at which they operate. This way, similar to the first test of the AA alkaline batteries, another test was performed but with a temperature lower than room temperature. In the graph of Figure 4.3.7 it is possible to see the SOC and the voltage of the batteries placed in a freezer at an approximate temperature of -18ºC with a constant resistance of 27 Ω and an initial current of 110 mA.

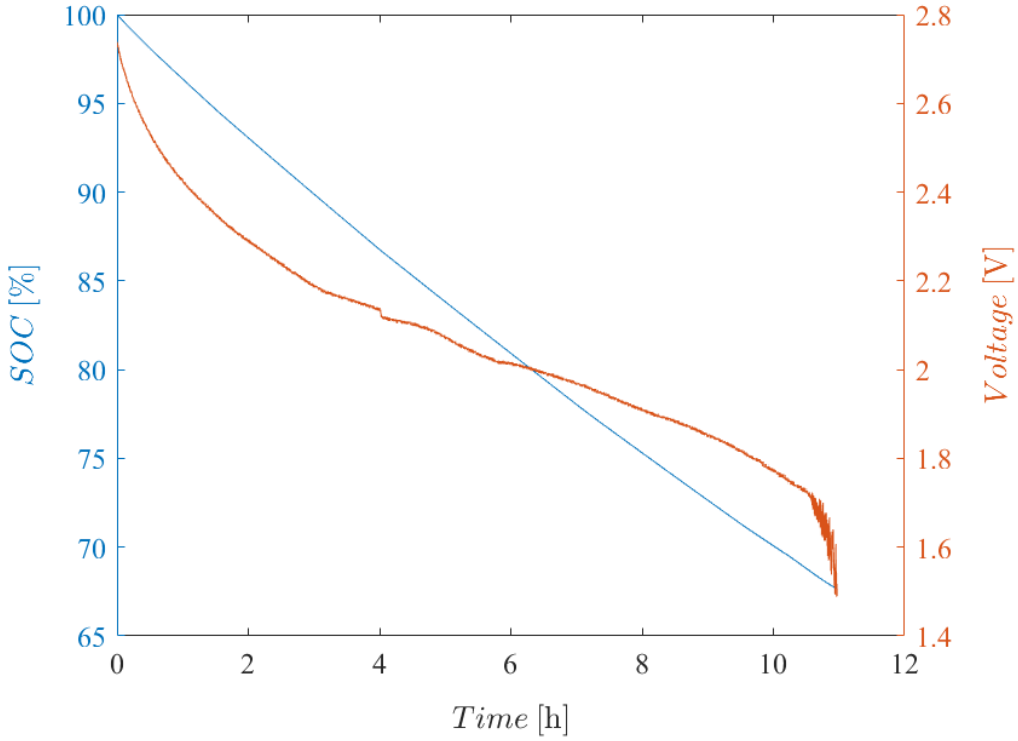

Figure 4.3.7 - SOC and voltage of two AA alkaline Energizer batteries with 27 Ω load impedance (-18ºC).

The batteries were securely sealed and placed inside a freezer until fully discharged with the remaining electronic equipment outside at a room temperature of 21°C. In those nearly eleven hours of measurement time, the SOC states the battery is at approximately 67% when it was starting to discharge irregularly. At that time, with an average discharge current of 81 mA, the discharged capacity, C_d, was,

$$C_d\ (\text{mAh}) \cong 81 \times 11 = 891\ \text{mAh}. \tag{41}$$

This is aligned with the SOC measurement since the discharged capacity is 30% of the total battery's capacity for which the SOC without current capacity should be around 70%. With current dependency, the SOC should be lower than this value which it validates it.

Then, illustrated in Figure 4.3.8, after the complete discharge at -18ºC, the batteries were placed one hour outside to room temperature and another test was made with the same two cells at room temperature to prove the charge remains inside the batteries.

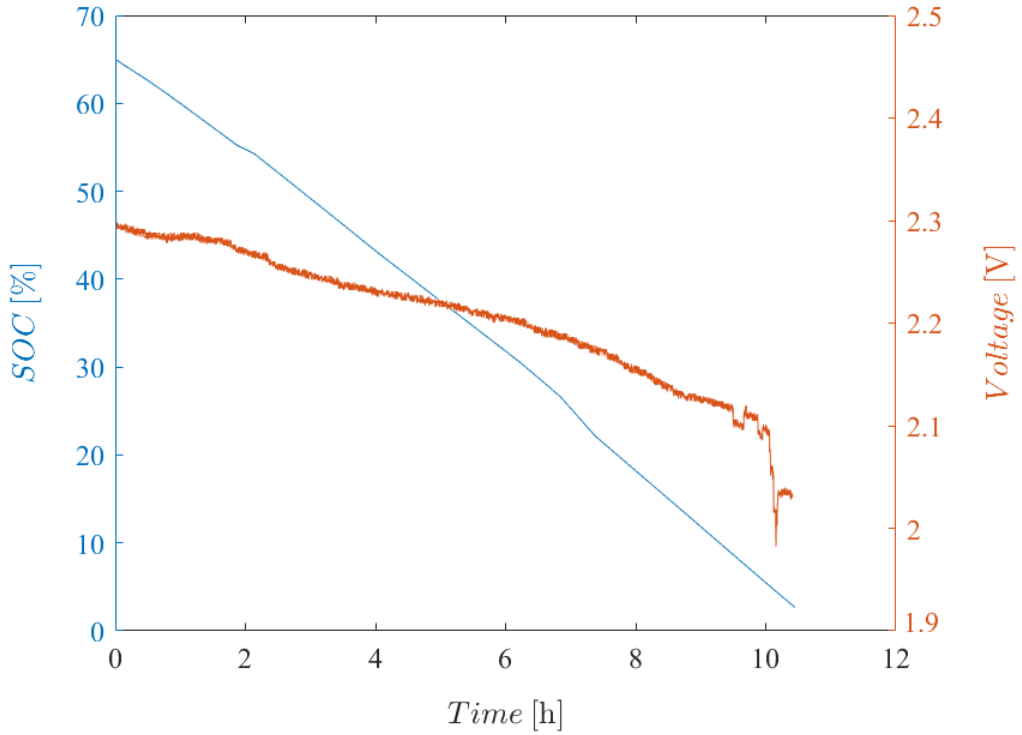

Figure 4.3.8 - SOC and voltage of two used AA alkaline Energizer batteries from -18ºC to 21ºC with 27 Ω load impedance (21ºC).

Comparing Figure 4.3.5 with Figure 4.3.7, having only changed the temperature of the batteries, it took almost the same time for the batteries to fully discharge at room temperature compared to the time at the freezer's temperature meaning it still had charge inside the battery. Thus, the dependency of the battery capacity on the temperature at which they operate is proven and, knowing that the voltage range of the batteries and the load resistance have not changed, it is possible to calculate the total battery capacity, C_B, after the exposer of these two temperatures until complete discharge,

$$C_B\ (\text{mAh}) = 891\ \text{mAh} + 81\ \text{mA} \times 10\ \text{h} \cong 1700\ \text{mAh}. \quad (42)$$

This means that at these operational temperature variations, the battery was not able to deliver the nominal charge due to the influence of low temperatures.

Afterwards, the tests on the AA lithium batteries were carried out, where it is expected that they will have a superior performance compared to alkaline batteries as occurred with the AAA cells. The AA lithium iron disulfide have around 3500 mAh instead of 2900 mAh of the alkaline batteries. The first test started with a resistance of 27 Ω powered by two AA batteries and, consequently, an initial current of 110 mA as shown in Figure 4.3.9.

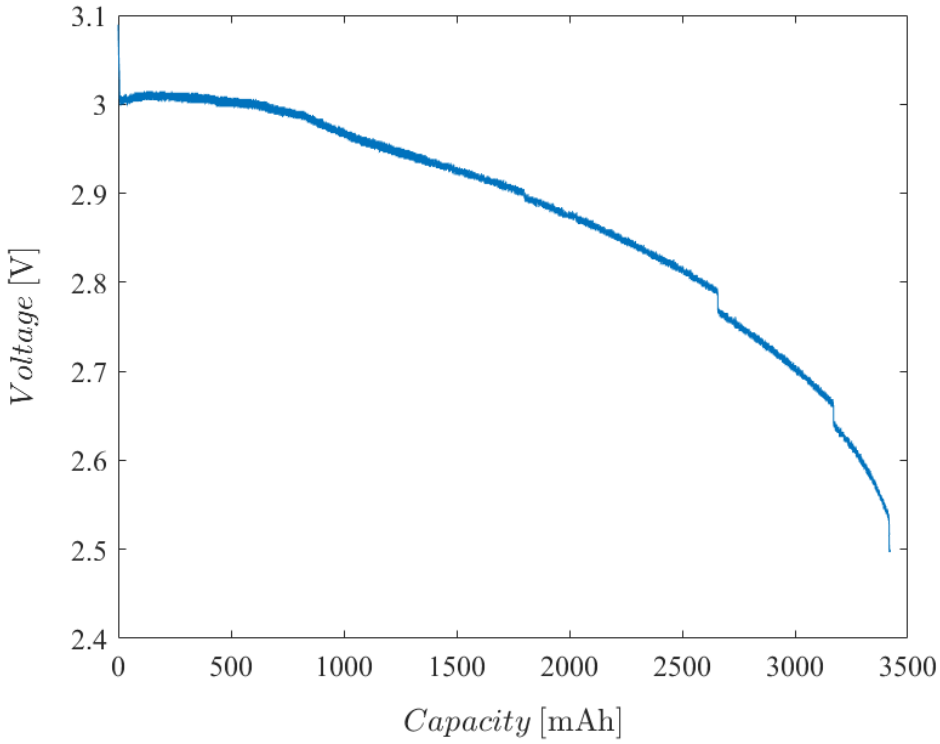

Figure 4.3.9 - SOC and voltage of two AA lithium Energizer batteries with 27 Ω load impedance (21ºC).

As with AAA lithium batteries, although there is no dependence of the battery's charge capacity on current, the current drops its value as the batteries' voltage decreases. Thus, the second test was performed with the same type of batteries but with a constant current of 110 mA as illustrated in Figure 4.3.10.

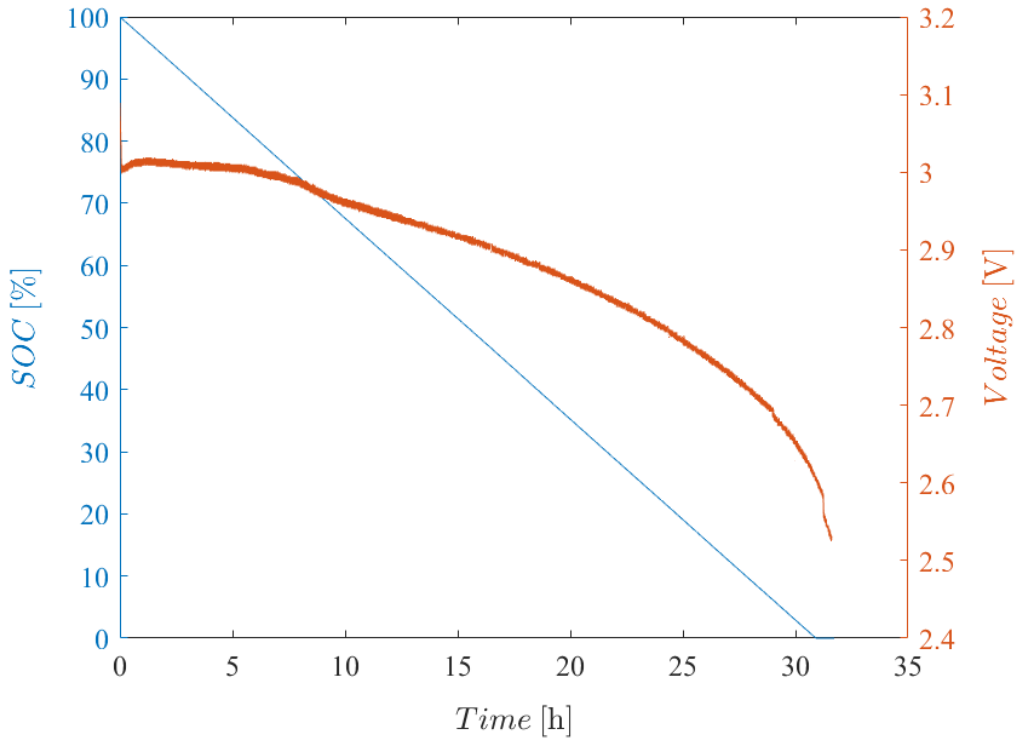

Figure 4.3.10 - SOC and voltage of two AA lithium Energizer batteries with 110 mA discharge current (21ºC).

As for temperature dependency, the Figure 4.3.11 illustrates the test made at -18ºC instead of the room temperature of 21ºC. As performed with AAA alkaline batteries, the lithium cells were placed in a plastic bag inside the refrigerator with this temperature and the other electronic components were set at room temperature.

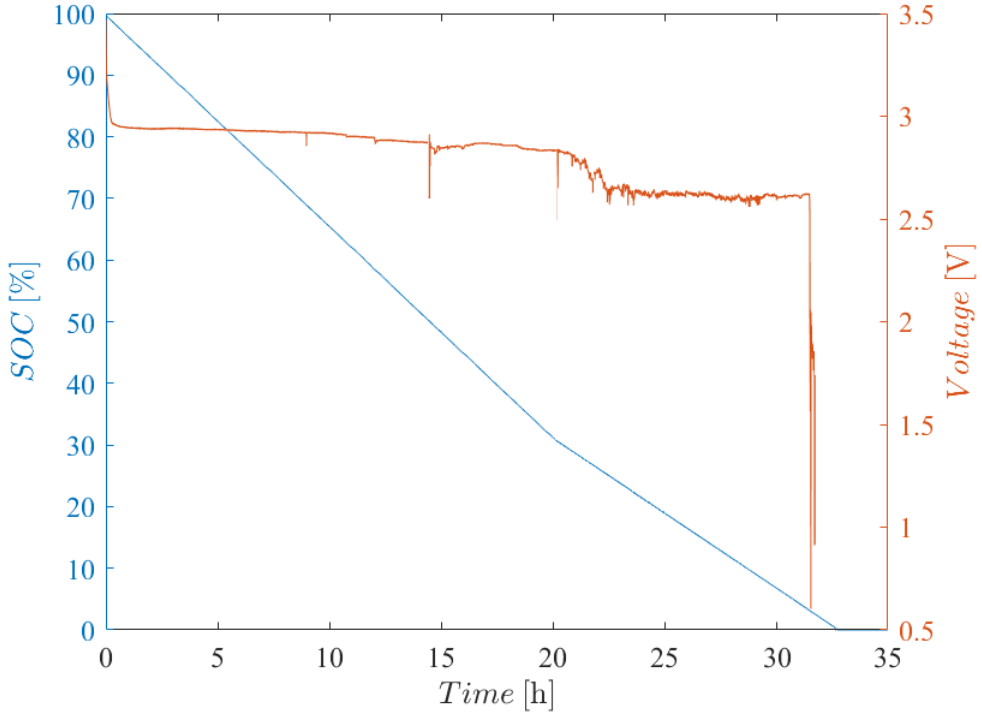

Figure 4.3.11 - SOC and voltage of two AA lithium Energizer batteries with a constant load impedance (-18ºC).

Differentely from alkaline, the capacity of these batteries is more tolerable to higher ranges of temperatures not having a significant difference between the room temperature performance as the tests with the AA alkaline batteries did. Therefore, for a device that a high discharge current, high ranges of temperature and low weighted battery are needed, the lithium iron disulfide batteries are recommended. Production and budget wise, the alkaline are much cheaper and safer than the lithium cells and recommended for these cases.

4.3.3 9 V Battery

Since AAA and AA batteries have the same voltage output, the commonly seen 9 V alkaline battery from Energizer was tested to study the differences between these types of batteries and the devices they were designed for. The 9 V rectangular shaped Energizer alkaline batteries have a nominal capacity of around 600 mAh with a maximum discharge current of 500 mA, but the capacity depends on the discharge current. Illustrated in Figure 4.3.12, a test was performed on this battery with a constant discharge current of 100 mA. With 500 mAh of capacity for 100 mA of constant current, the battery is expected to discharge completely in around five hours.

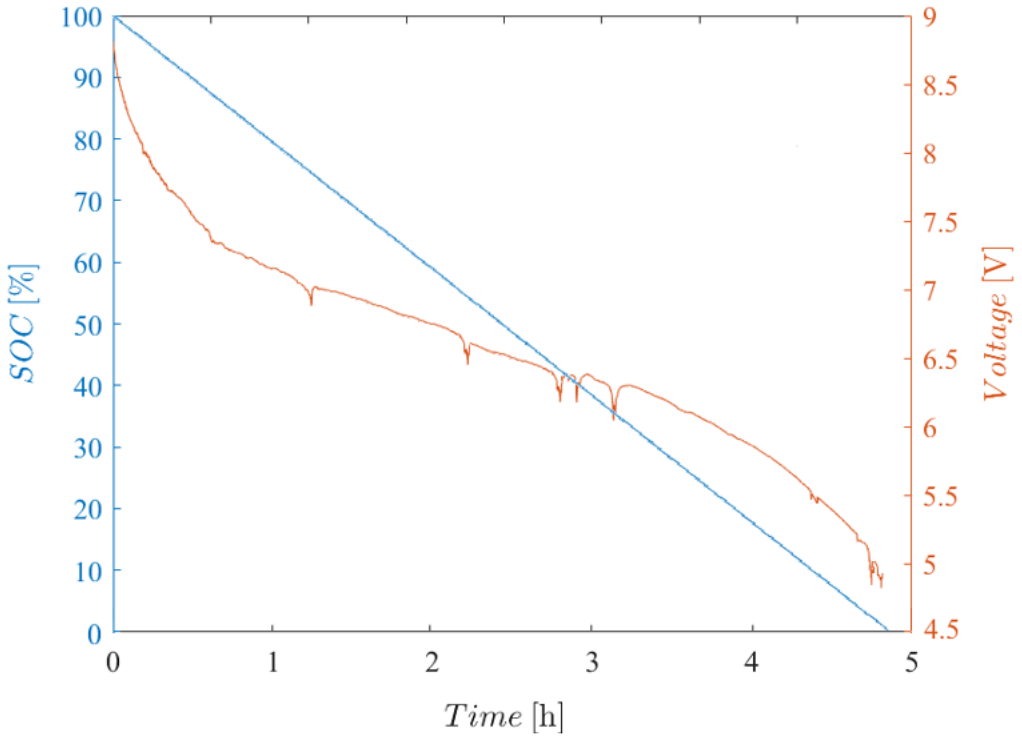

Figure 4.3.12 - SOC and voltage of a 9 V alkaline Energizer battery with a constant discharge current (21ºC).

Comparing the graph obtained with the data provided by the battery manufacturer illustrated in section 3.6, the time that the battery took to discharge completely with the discharge current of 100 mA was as mentioned. With this current, according to the manufacturer, the maximum capacity that the battery can provide is approximately 500 mAh, having obtained around 451 mAh in the test performed. This way, it is proven that the battery depends substantially on the current, having dropped about 25% of its nominal capacity with a current of 100 mA. As the voltage drops, the current drops aswell and the battery's voltage value increases since it depends on the discharing current too. Therefore, comparing with the other batteries previously studied, the oscilated orange line that represents the dropage of the battery's voltage only happens with this rectagular shaped power source since it has a higher voltage value.

4.4 Energy Efficiency

Energy efficiency is the concept of using less energy for the same outcome, in this case, integrating the current [27]. The ideal case would be if the circuit would have no energetic impact on the battery, but that is not possible. Therefore, the importance of this section is to reveal the efficiency of this circuit and the impact it has on the battery while measuring its SOC.

To determine the efficiency, it is necessary to calculate the power consumption for the maximum current measurement. As stated before, this project is only determined to measure currents in the range of 1 to 110 mA, so the current value used to calculate the energy efficiency is 110 mA. Afterwards, as illustrated in Figure 4.4.1, the power consumption of the circuit is analyzed by blocks.

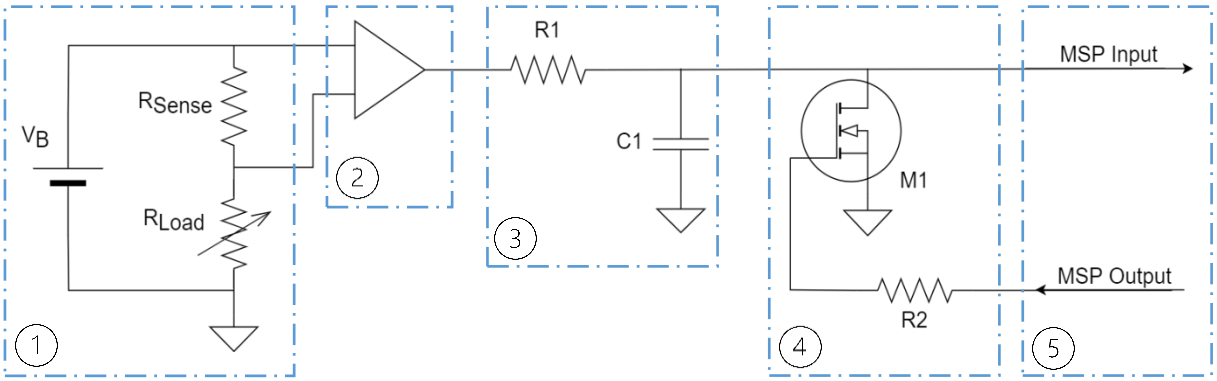

Figure 4.4.1 - Maximum power consumption by block.

In the first block, the sense resistor is the only component that belongs to the SOC power consumption, and it is calculated by,

$$P_{Rsense} = R \times I^2 = 0.27\ \Omega \times (110\ mA)^2 \cong 3.3\ mW. \quad (43)$$

On the second block, the Op-Amp is one of the components responsible for the efficiency of this circuit since it is the main reason that the sense resistors impedance may be as low as 270 mΩ. Without this component, the sense resistor would have to be at least twenty times its value and, as a result, this SOC measuring approach wouldn't be as accurate since the sense resistor would have a big influence on the charge's voltage.

To calculate the power consumption of the integrator, third block, it must be examined has a whole, this is, with the second and fourth block together. The first step is to calculate the charge of the capacitor until it reaches the comparison voltage of 1 V since the transistor from the fourth block discharges the capacitor once it reaches this value,

$$Q = C \times V = 330\ nF\ \times 1\ V = 330\ nC. \quad (44)$$

Then, the second step is to calculate the maximum current of the integrator which depends on the oscillating frequency. The higher the battery's discharging current, the higher the oscillating frequency, so for 110 mA the maximum frequency is equal to 54 Hz,

$$I_{max} = f \times Q = 54\ Hz\ \times 330\ nC < 18\ \mu A. \quad (45)$$

Even though the maximum Op-Amp's output voltage is 2.25 V, this component has a power source of 3.3 V. The final step is to calculate the maximum power consumption of these blocks by multiplying the maximum current with the Op-Amp's voltage supply,

$$P_{max} = I_{max} \times V = 18\ \mu A\ \times 3.3\ V < 59\ \mu W. \quad (46)$$

For the fourth block, the transistor's dynamic charge and discharge consumption is much lower than the previous blocks being almost insignificant for the energy efficiency calculation. As for the microcontroller it has a power consumption of 126 µA/MHz at 3.3 V, this is, for the SMCLK of 1.1 MHz used, the consumption of the microcontroller in active mode is 457 µW. Summing the power consumptions of all blocks, the maximum power consumption of the circuit is around,

$$P_{Total}\ (110\ mA) = 3.3\ mW\ +\ 59\ \mu W\ +\ 457\ \mu W\ \cong\ 3.8\ mW. \quad (47)$$

The circuit of this approach is energetically efficient since it consumes a maximum of 3.8 mW when discharging at 110 mA which is around 1% of the total 330 mW battery source.

On the other hand, for the minimum current value of 1 mA, the power consumption of the first block is approximately equal to,

$$P_{Rsense} = 270\ m\Omega \times (1\ mA)^2 \cong 270\ nW. \quad (48)$$

For the next blocks, the capacitor's charge remains the same but the value of the current changes for the different oscillating frequency. When discharging at 1 mA, the circuit's oscillating frequency is 34 Hz and the maximum current is,

$$I_{max} = 34\ Hz\ \times 330\ nC \cong 11\ \mu A. \quad (49)$$

Where the power consumption of the Op-Amp, integrator and transistor is approximately equal to,

$$P_{max} = 11\ \mu A \times 3.3\ V \cong 36\ \mu W. \quad (50)$$

And the total maximum power consumption of this circuit for 1 mA of discharge current is,

$$P_{Total}\ (1\ mA) = 270\ nW\ +\ 36\ \mu W + 457\ \mu W\ \cong\ 493\ \mu W. \quad (51)$$

In this case, when the battery is discharging 1 mA, the maximum power consumption of this SOC approach is 493 µW which exceeds the total 300 µW battery source.

However, in a real implementation of the circuit, there would be a power optimization on the components that were used inside the microcontroller in order to optimize its consumption. Thus, instead of the 126 µA/MHz, the power consumption of the fifth block would be a sum of the consumptions of the timer, counter, and comparator. The timer's consumption is around 5 µW/MHz and has the most power consumption compared to the other components since it was used 1.1 MHz of clock frequency for better count resolution. The other components and consumption on mathematical operations are almost insignificant when calculating the power consumption since they have a maximum frequency of 54 Hz instead of 1.1 MHz. Thus, in a real implementation the power consumption of the microcontroller would be approximately 18 µW instead of the 457 µW announced before.

5. Conclusions

Conclusions

5.1 Summary and Achievements

A SOC approach using the Coulomb counting method to measure current being discharged on batteries of IoT devices, is proposed in this work.

To validate the implemented SOC method, the circuit was attached to a DAQ that returned the instant voltage values of the batteries. These values were compared to the datasheets of the battery's manufacturer and, knowing the value of the sense resistor's impedance, it was possible to know the current being discharged by calculating the ratio of the measured voltage with the impedance value. Therefore, on some tests made, the desired discharging current was programmed using a programmable resistance as the simulating IoT device. This software development was achieved by measuring the OCV and then sending the resistance value in LabView to the programmable resistor to achieve the desired current set by the user at the built GUI program. The GUI was built to control the discharging current as well as to summarize the results using charts and virtual displays.

Although the Coulomb counting method was previously implemented, the approach used replaced the ADC component and was able to equally measure the current by integrating and relate it with the time between pulses not compromising the accuracy of the measurement, power consumption and production cost. By linking the SOC with the OCV measurements, it brings more assurance in the system through having more comparable data.

The achieved goals of the project in the validation results show the expected battery behaviors in different conditions and demonstrate the accuracy of the measurement with side-by-side graphical representation of the OCV of the developed circuit. Multiple tests on the batteries were made to have more conclusions about the capabilities of the Coulomb counting method.

The completed measurements in the validation results section of the purposed method show the success of the project's objectives on measuring current, especially for the efficiency, low cost production and for not noticeably influencing the battery's performance.

5.2 Future Work

In this section, the project's restrictions and constraints are addressed alongside with some improvements that can be made to enhance the global performance of the system.

- Some measurement's errors are due to some factors such as the cables used for connecting to the MSP430 and the electronic components and the size of the overall system. These could be reduced by manufacturing a PCB with all the components connected to each other minimizing the energy loss between these connections.
- Instead of depending on a computer, with a different processor, an LCD and a battery, this system could be portable and independent.
- With a different processor, more data could be added maximizing the accuracy of the current measured and additional processing performance could have been beneficial to minimize the overall processing time.
- This project's accuracy is limited to a current range of 1 to 110 mA measurement. Depending on the current, there could be more circuits in parallel with different integrating components that could improve the measurement with a wider current range.
- More acquisition samples require higher frequencies and more energy consumption. Reducing the frequency causes less acquisition samples and the project may not detect some current spikes. To improve the efficiency for constant current drainage, there could be an option where such frequency isn't required, and more energy could be spared.

References

[1] F. Gregorio, G. González, C. Schmidt, and J. Cousseau, “Internet of Things,” *Signals and Communication Technology*, 2020 (accessed Dec. 19, 2020).

[2] M. Batteries, “Alkaline vs. Lithium Batteries,” *Compare Alkaline Batteries with Lithium Batteries*. https://www.medicbatteries.com/alkaline-batteries-vs-lithium-batteries-compare-alkaline-lithium-alkaline-compared-to-lithium (accessed Dec. 20, 2020).

[3] P. Newswire, “Energizer® Sets GUINNESS WORLD RECORDS™ Title for the Longest-Lasting AA Battery,” *Energizer® Sets GUINNESS WORLD RECORDS™ Title for the Longest-Lasting AA Battery*, 2018. https://www.prnewswire.com/news-releases/energizer-sets-guinness-world-records-title-for-the-longest-lasting-aa-battery-300759658.html (accessed Aug. 20, 2021).

[4] B. Scrosati and J. Garche, “Lithium batteries: Status, prospects and future,” *Journal of Power Sources*, 2010. (accessed Aug. 20, 2021).

[5] B. a Battery, “Energizer Ultimate Lithium.” Accessed: Aug. 20, 2021. [Online]. Available: https://www.buyabattery.co.uk/brands/energizer-batteries/energizer-lithium-batteries.html.

[6] M. Forsyth and A. Bhatt, “How a battery works - Curious,” *www.science.org.au*, 2016. https://www.science.org.au/curious/technology-future/batteries (accessed Feb. 19, 2021).

[7] M. Precision, “What happens inside the rechargeable battery during charging and discharging? | Matsusada Precision ideal for,” 2020, Accessed: Jan. 06, 2021. [Online]. Available: https://www.matsusada.com/column/secondary-battery.html.

[8] REI, “How to Choose Batteries | REI Co-op.” https://www.rei.com/learn/expert-advice/batteries.html (accessed Jun. 29, 2021).

[9] T. Direct, “Lithium Battery Guide,” *torchdirect*. https://www.torchdirect.co.uk/lithium-battery-guide.html (accessed Jun. 29, 2021).

[10] E. Olivetti, J. Gregory, and R. Kirchain, “Life cycle assessment of alkaline batteries with focus on end-of-life disposal scenarios,” Massachusetts Institute of Technology, Materials Systems Lab, 2011. Accessed: Jan. 09, 2021. [Online]. Available: http://www.epbaeurope.net/documents/NEMA_alkalinelca2011.pdf.

[11] Newcastle Systems, “Lithium Ion vs Lithium Iron Batteries,” 2015. https://www.newcastlesys.com/blog/lithium-ion-vs-lithium-iron-batteries (accessed Jul. 06, 2021).

[12] Energizer, “Cylindrical Primary Lithium Handbook and Application Manual,” 2018. https://data.energizer.com/pdfs/lithiuml91l92_appman.pdf (accessed Jun. 29, 2021).

[13] P. Shen, M. Ouyang, L. Lu, J. Li, and X. Feng, “The co-estimation of state of charge, state of health, and state of function for lithium-ion batteries in electric vehicles,” *IEEE Transactions on Vehicular Technology*, 2018. (accessed Jan. 15, 2021).

[14] Electropaedia, “Battery and Energy Technologies,” *State of Charge (SOC) Determination*, 2005. https://www.mpoweruk.com/soc.htm (accessed Dec. 20, 2020).

[15] G. Keser, C. Roemmelmayer, and D. Gernert, “INDIRECT BATTERY PRESSURE MEASUREMENT,” Feb. 2018. (accessed Dec. 6, 2021).

[16] BehrTech, “6 Leading Types of IoT Wireless Technologies | BehrTech Blog,” *BEHRTECH Technologies Inc*. 2020, Accessed: Jan. 10, 2021. [Online]. Available: https://behrtech.com/blog/6-leading-types-of-iot-wireless-tech-and-their-best-use-cases/.

[17] Cecile Joannin, “Which types of batteries for your IoT devices? | Saft Batteries | We energize the world.,” 2005. https://www.saftbatteries.com/energizing-iot/types-batteries-iot-devices (accessed Jan. 10, 2021).

[18] J. Luo, Z. Cai, and G. Liu, “Research State of Charge Estimation Tactics of Nickel-Hydrogen Battery,” *Research State of Charge Estimation Tactics of Nickel-Hydrogen Battery*, 2010. https://ieeexplore.ieee.org/stamp/stamp.jsp?tp=&arnumber=5663056 (accessed Sep. 28, 2021).

[19] W.-Y. Chang, : M Brünig, and E. Di Nardo, “The State of Charge Estimating Methods for Battery: A Review Academic Editors,” Hindawi Publishing Corporation, 2013. doi: 10.1155/2013/953792.

[20] R. A. Cottis, “Coulomb Counting - an overview | ScienceDirect Topics,” *Electrochemical noise for corrosion monitoring*, 2008. https://www.sciencedirect.com/topics/engineering/coulomb-counting (accessed Feb. 19, 2021).

[21] Christiana Honsberg, “Battery Capacity | PVEducation,” 2016. https://www.pveducation.org/pvcdrom/battery-characteristics/battery-capacity (accessed Oct. 02, 2021).

[22] Energizer, “Energizer L91 - Ultimate Lithium,” 2009. https://energizer.lat/Brasil/produtos/energizer-ultimate-lithium-pilhas-aa/ (accessed Jul. 05,

2021).
[23] Energizer, “Product Datasheet Energizer E92,” *Prod. Datasheet*, pp. 1–2, 2014, Accessed: Jul. 16, 2021. [Online]. Available: https://data.energizer.com/. (accessed Aug. 20, 2021).
[24] I. S. B.V., “Temperature effects on batteries - Intercel Services B.V.” https://www.intercel.eu/frequently-asked-questions/temperature-effects-on-batteries/ (accessed Jul. 16, 2021).
[25] Energizer, “Product Datasheet Energizer LR6 AA Alkaline,” Accessed: Aug. 11, 2021. [Online]. Available: https://data.energizer.com/pdfs/alk-power-aa.pdf.
[26] Energizer, “Product Datasheet Energizer 6LR61 9V Alkaline,” Accessed: Aug. 11, 2021. [Online]. Available: https://data.energizer.com/pdfs/max-eu-9v.pdf.
[27] EESI, “Energy Efficiency | EESI,” *Environmental and Energy Study Institute*, 2020. https://www.eesi.org/topics/energy-efficiency/description (accessed Oct. 02, 2021).
[28] Quora, “Why cant you use a AAAA Battery instead of 2 AA Batteries.? - Quora.” https://www.quora.com/Why-cant-you-use-a-AAAA-Battery-instead-of-2-AA-Batteries (accessed Jun. 30, 2021).
[29] PushEvs, “Guoxuan unveils a cobalt-free LFP pouch battery cell with 212 Wh/kg - ?PushEVs.” https://pushevs.com/2021/01/10/guoxuan-unveils-a-cobalt-free-lfp-pouch-battery-cell-with-212-wh-kg/ (accessed Jul. 06, 2021).